J. Fluid Mech. (1992), *vol.* 238, *pp.* 371–404
Printed in Great Britain

Steady-state nonlinear internal gravity-wave critical layers satisfying an upper radiation condition

By KEVIN G. LAMB[1] AND RAYMOND T. PIERREHUMBERT[2]

[1] Department of Physics, Memorial University of Newfoundland, St. John's, Newfoundland, Canada A1B 3X7

[2] Department of the Geophysical Sciences, University of Chicago, 5734 Ellis Avenue, Chicago, IL, 60637 USA

(Received 16 February 1990 and in revised form 15 October 1991)

We consider the behaviour of an internal gravity wave encountering a critical level in a stratified fluid, assuming the critical-level flow to be dominated by nonlinear effects. The background flow is a shear layer, and the stratification is sufficiently strong to support wave propagation everywhere. Incident and reflected waves are permitted below the critical level, and a radiation condition is imposed far above it. For this geometry we construct, by a combination of asymptotic and numerical means, steady, nonlinear solutions, and discuss the associated transmission coefficients, reflection coefficients, phase shifts, and resonance positions when the system is forced from below.

The inviscid solutions we exhibit have continuous density and velocity everywhere, and so do not require the introduction of internal viscous boundary layers. Further, the streamlines bounding the recirculating cat's-eye regions have corners, just as in the unstratified case. For weak stratification, the transmitted wave is nearly as strong as the incident wave, and there is accompanying strong over-reflection. As the stratification increases, the critical level becomes a nearly perfect reflector. The amount of transmission depends on wave amplitude, and the sensitivity increases with increasing stratification.

There are regions of parameter space for which steady solutions could not be found. The critical-layer structure appears to break down by unbounded thickening when the stratification becomes too strong, suggesting that in these cases some neglected physical process must intervene to limit growth of the recirculating region.

1. Introduction

The fate of an internal gravity wave encountering a critical level (where the fluid speed equals the wave's phase speed) determines the behaviour of a considerable variety of important physical systems. For example, the amount of reflection and transmission largely determines the vertical distribution of gravity wave pseudo-momentum stress in the Earth's atmosphere, which greatly affects the mesospheric (Fritts 1984) and tropospheric (Palmer, Shutts & Swinbank 1986) circulations. The phase and strength of the reflected wave is also the key to predicting the occurrence of high-drag states of stratified flow over an obstacle (Peltier & Clark 1983; Bacmeister & Pierrehumbert 1988). Many examples of a similar nature could be cited.

The subject of internal gravity wave critical-level interactions has a long history, which is reviewed in some detail in Maslowe (1986). Understanding of the linear case

is essentially complete, owing to the work of Booker & Bretherton (1967) and followers. In essence, the incident wave is largely absorbed whenever the stratification is much in excess of that required to render the flow stable to Kelvin–Helmholtz instability. For the analogous unstratified problem of a barotropic Rossby wave impinging on a critical level, the transient and steady-state nonlinear behaviour is thoroughly understood as well (see for example Killworth & McIntyre 1985). After a sufficiently long time the critical level becomes a perfect reflector. The nonlinear stratified problem is much harder, owing to the lack of a conserved scalar vorticity. In the present work, we adopt the approach of constructing steady solutions to the nonlinear problem satisfying plausible physical constraints. It is anticipated that these represent end states of the long-term evolution of the initial-value problem, but the time evolution is not explicitly treated. This approach is similar to that employed to good effect by Benney & Bergeron (1969) in the first treatments of the nonlinear unstratified case. The programme we have undertaken complements asymptotic approaches such as that of Brown & Stewartson (1980), which compute the time evolution in detail, but cannot pass to the infinite time limit when there is appreciable stratification. It should be emphasized that although we invoke viscous arguments twice in order to close the problem, the solutions we construct are solutions of the inviscid equations and have discontinuities of vorticity across the cat's-eye boundaries. This does not contradict the results of other authors (e.g. Haberman 1972; Brown & Stewartson 1978) who show that the vorticity diffuses out until the mean flow is modified. Our steady inviscid states should be viewed as steady on a timescale which is small compared to the viscous timescale. The mean flows of our solutions are modified mean flows of unknown initial states.

Our work follows directly in the tradition of Maslowe (1972, 1973) and Graham (1982), but with fewer restrictions on geometry. Specifically, the stratification is strong enough to support wave propagation everywhere, and not just in the vicinity of the critical layer. This permits us to stipulate forcing by flow over an obstacle well below the critical layer, and to impose a radiation condition far above the critical layer. Our solutions thus have fewer built-in symmetries than previous solutions, and are closer to the physical situations of interest in atmospheric problems. This configuration also allows us to evaluate reflection and transmission coefficients. The asymptotic critical-layer equations that are the basis for our study are precisely those derived by Maslowe, but the numerical methods used to solve them, the boundary conditions imposed, and the physical constraints required to be satisfied are all very different. Most notably, we make use of a 'torque condition' to determine the vorticity in the recirculating cat's-eye regions, and allow a shift in the position of the critical layer; the latter allows us to construct solutions which have no velocity discontinuity at the cat's-eye boundaries, and which therefore do not require the introduction of viscous boundary layers. Moore & Saffman (1982) also constructed solutions with continuous velocity and discontinuous vorticity using a considerably different approach when they considered finite-amplitude waves in an unstratified fluid. Like Graham they assumed that the vorticity distribution was unaltered during the evolution to the final steady state. In place of our torque condition they determined the vorticity inside the cat's-eyes by assuming that the total vorticity of the final state was the same as for the initial state. For a stratified fluid, however, density gradients can generate vorticity making this assumption questionable. We also take the point of view that the evolution to a final steady state will involve turbulent mixing, a further reason making such assumptions inappropriate.

The mathematical formulation of the problem is described in §2; here we also

briefly recapitulate the derivation of Maslowe's asymptotic equations, which establishes notation. Some basic properties of the equations are derived in §3.1, and properties of solutions with continuous velocity everywhere and the torque and corner conditions are discussed in §3.2. A numerical method for computing these is given in §4.1; general features of the solutions are illustrated through a detailed case study described in §4.2, while the broader dependence of reflection coefficients, transmission coefficients, resonance positions and cat's-eye shapes on the controlling parameters are taken up in §4.3 and 4.4. Our principal conclusions are summarized in §5.

As in most previous studies we restrict attention to two-dimensional waves which are periodic in the streamwise direction. The case of waves forced by a localized obstacle in a horizontally unbounded medium is of equal physical interest, but will be deferred to future work. We caution that localized waves are apt to behave rather differently, owing to the fundamental difference in streamline geometry. A less important restriction is our concentration on incompressible flow; compressibility is unlikely to affect features due to the critical level, as its thickness will typically be much less than a scale height in terrestrial circumstances.

2. Formulation of the problem

Consider a two-dimensional incompressible non-rotating flow governed by the Boussinesq equations. Let the horizontal and vertical coordinates and velocities be (x, z) and (u, w) respectively, while ρ is the density variation with respect to a constant value non-dimensionalized to 1.

Consider a mean horizontal flow of the form

$$(u, w, \rho) = (\bar{U}(z), 0, \bar{\rho}(z)) \tag{2.1}$$

which has a single zero wind line at $z = 0$ with $\bar{U}'(0) > 0$ and $\bar{\rho}'(z) < 0$ (primes denote differentiation with respect to z). In addition, $\bar{U}$ approaches a constant value far above the zero wind line. This basic state is an exact solution of the inviscid Boussinesq equations. The non-dimensionalization and choice of the representative density value has been done so that $\bar{U} = 1$ far above the critical layer and

$$\lim_{z \to 0^+} (\bar{U}(z), \bar{U}'(z), \bar{\rho}(z), \bar{\rho}'(z)) = (0, 1, 0, -1). \tag{2.2}$$

Suppose a perturbation is introduced below the zero wind line via a solid boundary at

$$z = -H + \epsilon h(x), \tag{2.3}$$

where ϵ is a small parameter controlling the amplitude of the variations in the boundary. Assume that after a period of time the flow settles into a quasi-steady state, that is, a state which is steady on timescales much less than the viscous timescale. These quasi-steady states, henceforth referred to as steady states, are steady-state solutions of the inviscid equations. The goal of this paper is to establish the properties of possible steady states, and to construct explicit examples. Only solutions periodic in x are considered. Viscous effects are brought in only to close the inviscid problem.

It has been known since Bretherton (1966) that steady, linear inviscid theory breaks down near a critical level, which in this case is at the zero wind line $z = 0$. Solutions can be continued through the singular region only through the addition of nonlinear or viscous effects. For the geophysical applications we have in mind it is the former that are of primary interest.

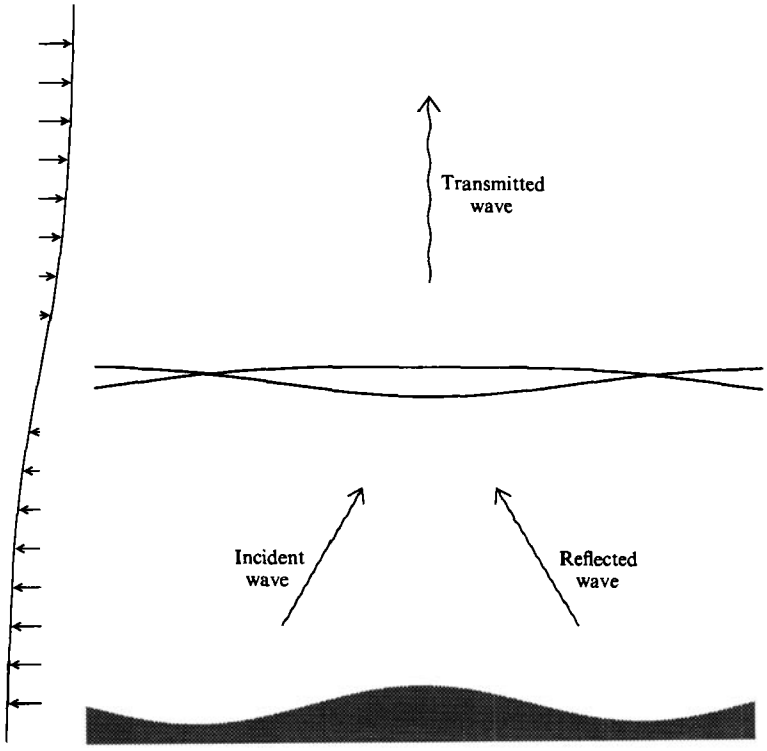

FIGURE 1. This schematic diagram shows the general form of the solution forced by flow over a hill. The arrows on the left represent the mean flow. Some of the incident wave is reflected and some is transmitted by the cat's-eyes.

The region of the flow $z > -H + \epsilon h(x)$ is naturally separated into three regions. In a thin neighbourhood of the critical level the flow is nonlinear. Above and below it are two regions where, because of the small amplitude of the forcing, the flow may be taken to be linear. The final steady state will have incident and reflected waves in the lower linear layer. Above the nonlinear critical layer the flow is assumed to be stratified so that the waves escape to $+\infty$. An upper radiation condition is applied so that only upward-propagating (transmitted) waves are present. Previous authors have taken the fluid to be stratified in only a finite neighbourhood of the nonlinear critical layer so that only trapped modes were possible. The problem considered here has more asymmetry about $z = 0$ because of the different waves in the two linear layers. A schematic of the situation is shown in figure 1. The nonlinear critical layer consists of regions of open streamlines and regions of closed streamlines (figure 2), the latter being commonly called cat's-eyes.

In relating the steady solutions to the outcome of an initial-value problem, it may be reasonable to assume that within the linear regions these profiles are little changed from the initial state; near the critical layer, however, strong mean flow modifications are expected and there is no reason to expect the ultimate steady profile to resemble the initial one particularly. Let the mean horizontal velocity and density of the perturbed steady state in the upper and lower linear layers be $\bar{U}_{u,1}(z)$ and $\bar{\rho}_{u,1}(z)$. It will be stipulated that $\bar{U}_{u,1}(z)$ and $\bar{\rho}'_{u,1}(z)$ are all constant far from the critical layer so that upward- and downward-propagating waves can be unambiguously distinguished. A slight modification of the non-dimensionalization allows us to make (2.2) hold for $\bar{U}_u$ and $\bar{\rho}_u$.

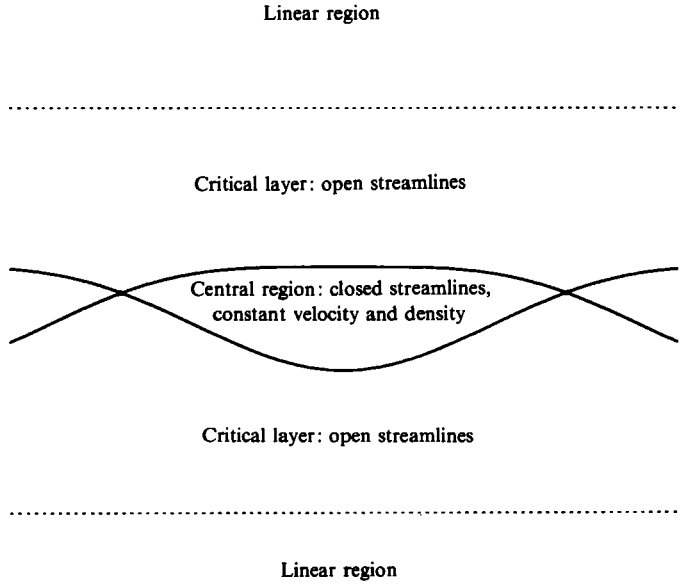

FIGURE 2. This schematic diagram shows an expanded view of the nonlinear critical layer. It consists of regions of open streamlines and a central region of closed streamlines where the density and vorticity are constant.

In terms of the stream function the governing equations in non-dimensional form are

$$\frac{\partial}{\partial t}\nabla^2\Psi + J(\nabla^2\Psi, \Psi) = \overline{Ri}\,\rho_x + \nu\nabla^2\nabla^2\Psi, \tag{2.4a}$$

$$\frac{\partial\rho}{\partial t} + J(\rho, \Psi) = \frac{\nu}{Pr}\nabla^2\rho, \tag{2.4b}$$

where
$$J(A,B) = A_xB_z - A_zB_x, \tag{2.4c}$$

and
$$(u, w) = (\Psi_z, -\Psi_x). \tag{2.4d}$$

Here $\overline{Ri}$ is the limiting value of the Richardson number of the mean flow in the upper linear layer as $z \to 0$, ν is the reciprocal of the Reynolds number and Pr is the Prandtl number.

In the linear regions the appropriate asymptotic expansion is

$$\Psi = \bar{\Psi} + \epsilon\Psi^{(1,0)} + \epsilon^2\Psi^{(2,0)} + \ldots + \nu(\Psi^{(0,1)} + \epsilon\Psi^{(1,1)} + \ldots) + \nu^2(\Psi^{(0,2)} + \epsilon\Psi^{(1,2)} + \ldots) + \ldots, \tag{2.5a}$$

$$\rho = \bar{\rho} + \epsilon\rho^{(1,0)} + \epsilon^2\rho^{(2,0)} + \ldots + \nu(\rho^{(0,1)} + \epsilon\rho^{(1,1)} + \ldots) + \nu^2(\rho^{(0,2)} + \epsilon\rho^{(1,2)} + \ldots) + \ldots, \tag{2.5b}$$

where $\bar{\Psi} = \int^z \bar{U}(z')\,dz'$ and $\bar{\rho}$ represent the mean values. Substituting into the governing equations we find that, for a steady-state solution, the $O(\epsilon)$ terms are given by

$$\rho^{(1,0)} = \frac{\bar{\rho}'}{\bar{U}}\Psi^{(1,0)}, \tag{2.6a}$$

$$\bar{U}^2\nabla^2\Psi^{(1,0)} - \bar{U}\bar{U}''\Psi^{(1,0)} + N^2(z)\Psi^{(1,0)} = 0, \tag{2.6b}$$

where $N^2(z) = -\overline{Ri}\,\bar{\rho}'(z)$ is the Boussinesq approximation of the buoyancy frequency.

Writing $\Psi^{(1,0)}$ as $\phi(z)e^{ikax}$ leads to the well known Taylor–Goldstein equation for the vertical structure

$$\phi''+\left[\frac{N^2(z)}{\bar{U}^2(z)}-\frac{\bar{U}''(z)}{\bar{U}(z)}-k^2\alpha^2\right]\phi=0. \tag{2.7}$$

As is well known (see for example Maslowe 1972), near the point z_c where $\bar{U}=0$ the solution to (2.7) has the singular behaviour

$$\phi\sim A(z-z_c)^{\frac{1}{2}+i(R_c-\frac{1}{4})^{\frac{1}{2}}}+B(z-z_c)^{\frac{1}{2}-i(R_c-\frac{1}{4})^{\frac{1}{2}}} \quad \text{as} \quad z\to z_c, \tag{2.8}$$

where $R_c=N^2(z_c)$. The asymptotic expansion breaks down when $|z-z_c|=\epsilon^\gamma$, where

$$\gamma^{-1}=\begin{cases}\frac{3}{2} & \text{if} \quad R_c>\frac{1}{4};\\ \frac{3}{2}+(\frac{1}{4}-R_c)^{\frac{1}{2}} & \text{if} \quad R_c<\frac{1}{4};\end{cases} \tag{2.9}$$

at which point

$$\left.\begin{aligned}O(\bar{\Psi})=O(\epsilon\Psi^{(1,0)})=O(\epsilon^2\Psi^{(2,0)})=\ldots=\epsilon^{2\gamma},\\ O(\bar{\rho})=O(\epsilon\rho^{(1,0)})=O(\epsilon^2\rho^{(2,0)})=\ldots=\epsilon^{\gamma}.\end{aligned}\right\} \tag{2.10}$$

A new set of variables for the thin critical layer are introduced via

$$\Phi=\epsilon^{-2\gamma}\Psi, \quad \Theta=\epsilon^{-\gamma}\rho, \quad \zeta=\epsilon^{-\gamma}z. \tag{2.11}$$

Substituting these changes into the governing equations gives the rescaled governing equations used in the nonlinear critical layer. They are

$$J(\Phi_{\zeta\zeta},\Phi)=\overline{Ri}\Theta_x+\lambda\Phi_{\zeta\zeta\zeta\zeta}-\epsilon^{2\gamma}J(\Phi_{xx},\Phi)+2\lambda\epsilon^{2\gamma}\Phi_{xx\zeta\zeta}+\lambda\epsilon^{4\gamma}\Phi_{xxxx}, \tag{2.12a}$$

$$J(\Theta,\Phi)=\frac{\lambda}{Pr}\Theta_{\zeta\zeta}+\lambda\frac{\epsilon^{2\gamma}}{Pr}\Theta_{xx}, \tag{2.12b}$$

where the Jacobian is now with respect to x and ζ. The small parameter $\lambda=\nu/\epsilon^{3\gamma}$ is the cube of the ratio of the thickness of the viscous layer ($\nu^{\frac{1}{3}}$) to the thickness of the nonlinear layer (ϵ^γ). It is assumed to be much smaller than 1, because we are interested in the nonlinearity-dominated regime.

Let $\phi^{(0)}$ and $\Theta^{(0)}$ be the leading-order terms. They are governed by

$$J(\Phi^{(0)}_{\zeta\zeta},\Phi^{(0)})=\overline{Ri}\,\Theta^{(0)}_x, \quad J(\Theta^{(0)},\Phi^{(0)})=0, \tag{2.13}$$

which have the general solution

$$\Theta^{(0)}=F(\Phi^{(0)}), \quad \Phi^{(0)}_{\zeta\zeta}=G(\Phi^{(0)})-\overline{Ri}\,\zeta F'(\Phi^{(0)}).$$

Note that the density is constant along streamlines but the vorticity $\Phi^{(0)}_{\zeta\zeta}$ is not.

The arbitrary functions F and G are determined by assuming horizontal periodicity and invoking a viscous secularity condition (Maslowe 1972) which requires that the equations for the leading-order viscous terms have a solution periodic in x. This approach is chosen over the alternative method used by other authors (Graham 1982; Moore & Saffman 1982) of assuming that the functions F and G are the same as those of the basic state. Because density gradients can generate vorticity and because of the likelihood of turbulent mixing during the evolution to a final steady state, the use of the viscous secularity condition seems more physically realistic. The equations are obtained in their simplest form by first rewriting the governing equations using $(x,\Phi^{(0)})$ as independent variables. This procedure yields equations for F and G which involve two constants whose values are determined by the match to the linear regions (details of this are given by Maslowe 1972). Combining these

with equations for $\zeta(x, \Phi^{(0)})$ and $u(x, \Phi^{(0)})$ gives a complete set of equations for the flow in the two regions of open streamlines adjacent to the linear regions. They are valid only in regions where the flow is smooth and the velocity is non-zero.

The complete set of equations for the nonlinear open-streamline regions is

$$\zeta_\Phi = \frac{1}{u} \tag{2.15}$$

$$u_\Phi = \frac{G - \overline{Ri}\,\zeta F'}{u} \tag{2.16}$$

$$F' = A \Big/ \int_0^L u \, \mathrm{d}x \tag{2.17}$$

$$G' = \frac{\overline{Ri}\,F'^2}{A}\left[L - \frac{1}{Pr}\left[I_3 - \frac{(1-Pr)}{A} F' I_1 I_2\right]\right] \tag{2.18}$$

where the superscripts have been dropped and

$$A = \lim_{z \to z_c} \bar{\rho}'_\alpha(z) L \quad (\alpha = \mathrm{l}, \mathrm{u} \text{ as appropriate}), \tag{2.19}$$

$$I_1 = \int_0^L \zeta u \, \mathrm{d}x, \tag{2.20}$$

$$I_2 = \int_0^L \frac{G - \overline{Ri}\,\zeta F'}{u} \mathrm{d}x, \tag{2.21}$$

$$I_3 = \int_0^L \zeta \left(\frac{G - \overline{Ri}\,\zeta F'}{u}\right) \mathrm{d}x. \tag{2.22}$$

Note that the constant A will in general have different values above and below the critical layer. L is the horizontal period.

The numerical solution of this system is evaluated by discretizing the x-dependence on a uniform grid, employing second-order centred differences for the horizontal derivatives. If there are P grid points in the x-direction the problem reduces to $2P+2$ coupled nonlinear ordinary differential equations which are solved by a fourth-order Runge–Kutta method. The system can be solved only up to the streamline along which u first has a zero value.

3. Structure of the critical layer

There is no guarantee that the solution to a nonlinear boundary-value problem (if, indeed, it exists at all) is unique; largely inviscid problems such as the one at hand are prone to a particularly high degree of degeneracy. In order to select a solution, auxiliary physical assumptions must be invoked, with the understanding that the worth of these assumptions must ultimately be probed through numerical or asymptotic treatment of the nonlinear initial-value problem. The current understanding of unstratified critical levels has been attained through a similar sequence of events.

Equations (2.15)–(2.22) appear to uniquely determine the solution within the region of open streamlines (where u is non-zero), but in fact can support a density discontinuity and corresponding velocity discontinuity across any streamline; we shall assume that no such discontinuities exist, although we allow discontinuities

across the cat's-eye boundaries. Within the cat's-eyes, where (2.15)–(2.22) are invalid, we assume the density and vorticity to be constant. The Prandtl–Bachelor theorem is commonly invoked to support assumptions of this type, but strict application of the theorem is precluded by the stagnation streamlines bounding the cat's-eyes (allowing tracer to ultimately escape to the open-streamline region). Nevertheless, the likelihood of rapid mixing due to shear dispersion (as in Killworth & McIntyre 1985) and turbulence driven by overturning density contours makes the assumption plausible.

It will be shown that given the above assumptions the problem becomes one of determining the value of seven different constants. However, barring extraordinary circumstances, the solutions must have continuous density and velocity across the cat's-eye boundaries (Lamb 1989). This reduces the problem to one of determining three different constants. These solutions should be regarded as merely one member of a continuous family of solutions. More general solutions, in which for example the mixed region extends beyond the cat's-eyes, may be equally plausible. Such enlargements of the parameter space would be best effected in the light of guidance from simulations of the full initial-value problem. In any event, it may be hoped that gross characteristics such as reflection and transmission coefficients are not too sensitive to the details of the flow in the critical layer.

3.1. *Basic properties*

Let $Z_{\mathrm{u}}(x)$ and $Z_{\mathrm{l}}(x)$ be the upper and lower boundaries of the cat's-eyes. In general assume that the density ρ and horizontal velocity u may be discontinuous at these boundaries. For any flow quantity Q let

$$Q_{\alpha}^{+,-}(x) = \lim_{\zeta \to Z_{\alpha}^{+,-}(x)} Q(x,z) \quad (\alpha = \mathrm{u}, \mathrm{l}). \tag{3.1}$$

Also let

$$\rho_{\mathrm{l}} = \lim_{\zeta \to Z_{\mathrm{l}}^{-}(x)} \rho(x,\zeta), \quad \rho_{\mathrm{u}} = \lim_{\zeta \to Z_{\mathrm{u}}^{+}(x)} \rho(x,\zeta) \tag{3.2a, b}$$

be the fluid densities immediately below and above the cat's-eyes. Finally let ρ_0 and N_0 be the constant values of the density and the vorticity inside the cat's-eyes, so that

$$(\rho(x,\zeta), \Phi_{\zeta\zeta}(x,\zeta)) = (\rho_0, N_0) \quad \text{for} \quad Z_{\mathrm{l}}(x) < \zeta < Z_{\mathrm{u}}(x). \tag{3.3}$$

Now consider the interior of the cat's-eyes. The boundaries $Z_{\mathrm{l}}(x)$ and $Z_{\mathrm{u}}(x)$ meet at some point (x_0, ζ_0). Thus the stream function necessarily has the same value, Φ_0 say, on both boundaries. The general solution in the cat's-eyes can then be written as

$$\Phi - \Phi_0 = \tfrac{1}{2} N_0 \zeta^2 + a(x)\zeta + b(x). \tag{3.4}$$

Setting the right-hand side of (3.4) to zero and solving for ζ gives the lower and upper boundaries in terms of $a(x), b(x)$ and N_0 as

$$Z_{\mathrm{l}} = \frac{-a(x) - [a^2(x) - 2N_0 b(x)]^{\frac{1}{2}}}{N_0} \tag{3.5a}$$

and

$$Z_{\mathrm{u}} = \frac{-a(x) + [a^2(x) - 2N_0 b(x)]^{\frac{1}{2}}}{N_0}. \tag{3.5b}$$

Evaluating the horizontal velocity Φ_{ζ} along the bounding contours shows that

$$u_{\mathrm{l}}^{+}(x) = -u_{\mathrm{u}}^{-}(x) = -[a^2(x) - 2N_0 b(x)]^{\frac{1}{2}}. \tag{3.6}$$

Hence

$$Z_l = Z_u - \frac{2u_u^-(x)}{N_0}. \tag{3.7}$$

A relationship between the jumps of the density and horizontal velocity across the bounding contours can be obtained by considering the Bernouilli constant $p+\frac{1}{2}u^2+\overline{Ri}\rho\zeta$. Continuity of pressure then gives

$$u_l^{+^2}(x) = u_l^{-^2}(x) + 2\overline{Ri}\,(\rho_l - \rho_0)\,Z_l(x) + C_l, \tag{3.8a}$$

$$u_u^{+^2}(x) = u_u^{-^2}(x) + 2\overline{Ri}\,(\rho_0 - \rho_u)\,Z_u(x) + C_u \tag{3.8b}$$

for some constants C_l and C_u.

The problem of determining the solution in the critical layer can be reduced to one of determining a number of constants. Suppose the solution above the region of closed streamlines is known, i.e. $\zeta(x,\Phi)$, $u(x,\Phi)$, $G(\Phi)$ and $F(\Phi)$ have been solved up to the critical streamline on which u first vanishes, where, say, $\Phi = \Phi_0$. Let Φ_u be the value of the stream function on the contour defining the lower boundary of the cat's-eye region. This streamline need not be the one on which u first vanishes. Indeed, Maslowe (1972) and Graham (1982) chose to begin the cat's-eye region before the critical streamline was reached, evidently in an attempt to fix the position of this region at $z = 0$, where the undisturbed wind profile has its zero. Given that there is ample opportunity for mean flow changes in the course of evolution from the undisturbed state, there seems to us little reason to impose such a constraint. We will choose $\Phi_u = \Phi_0$, and thus not begin the cat's-eye region until forced to do so by the breakdown of (2.15)–(2.18). Once the value of Φ_u is chosen, $Z_u(x)$, $u_u^+(x)$ and ρ_u are known.

The jump condition (3.8*a*) shows that, given the density ρ_0 in the central region, $u_u^-(x)$ is determined since C_u is determined on the basis that u_u^- has a minimum value of zero (u_u^- being $\geqslant 0$). The point at which this occurs is where $Z_l(x)$ and $Z_u(x)$ meet.

Equations (3.6) and (3.7) give u_l^+ and then $Z_l(x)$ once N_0 is known. Knowledge of ρ_l and C_l then determines $u_l^-(x)$. Finally the flow field below $Z_l(x)$ needs to be determined. $Z_l(x)$, $u_l^-(x)$ and ρ_l provide initial conditions for the equations for ζ, u and F. An initial condition G_l for G is still needed. Also, recall that the equation for F involves a constant A which may have different values A_u and A_l above below the critical layer. Because of the large amount of mixing due to such nonlinear effects as wave breaking it is not clear what the relationship between A_u and A_l should be.

3.2. *Continuous solutions*

The problem thus far is to determine the values of the seven constants Φ_u, ρ_0, N_0, ρ_l, C_l, G_l and A_l. The most physically interesting solutions are those for which the velocity, and hence the density, is continuous everywhere. This restraint dictates that $\Phi_u = \Phi_0$, in order to prevent a velocity discontinuity across the point of contact of the lower and upper cat's-eye boundaries. It further fixes the values of ρ_0, ρ_l, and C_l. Only the values of three constants N_0, G_l and A_l remain to be determined.

The first question to be considered is the behaviour of $Z_u(x)$ at x_0, the x-coordinate of the point on $Z_u(x)$ where the horizontal velocity is zero. In particular, is $Z_u'(x)$ continuous at x_0 or not? If it is not continuous the boundary has a corner at x_0. This property is of some interest, as the results reviewed in Maslowe (1986) would seem to imply that lack of corners in the cat's-eye boundaries is a feature distinguishing the stratified from the unstratified case.

A consideration of the unstratified problem, for which the leading-order problem

can be solved analytically, is instructive at this point. For an unstratified flow exact analytic solutions of the nonlinear critical-layer equations can be obtained. It is well known that when there is a single harmonic in the linear layers there is a jump in the slopes of the cat's-eye boundaries at the point where they meet (e.g. Benney & Bergeron 1969). There is also, however, a family of solutions for which $Z_l(x)$ and $Z_u(x)$ are smooth.

For the unstratified problem the leading-order solution in the critical layer is given by

$$\Phi_{\zeta\zeta} = uu_\Phi = G(\Phi).$$

Applying the inviscid secularity conditions (identical to the one for the stratified problem) shows that G must be constant. That is, the unstratified problem can be obtained from the stratified problem simply by setting $\overline{Ri}$ equal to zero. Hence the critical-layer solution is

$$\Phi = \tfrac{1}{2}\bar{u}_c'\,\zeta^2 + b(x), \tag{3.9}$$

where $b(x)$ is determined by the stream function in the linear layers. The shape of the streamlines is given by solving for Z in terms of ϕ giving

$$Z = \pm(2/\bar{u}_c')^{\frac{1}{2}}[\Phi - b(x)]^{\frac{1}{2}}.$$

The cat's-eye boundaries are obtained by setting $\Phi = \Phi_0$, where Φ_0 equals the maximum value of $b(x)$. If $b(x)$ consists of a single harmonic, as is usually assumed, we find that Z_l and Z_u have corners at the points where they meet. There is, in addition, a class of solutions of which Z_l and Z_u are smooth, namely when $\phi_0 - b(x) = a^2(x)$ with $a(x) \geqslant 0$ or $a(x) \leqslant 0$. Such a solution requires a condition between the leading harmonic and the higher harmonics to be met.

There are no exact solutions for the stratified problem. Note however that, at the point where $Z_l(x)$ and $Z_u(x)$ meet, the vertical density derivative is zero since $\rho\zeta = u\rho_\Phi$ and $u = 0$ and $\rho_\Phi = F'$ is finite. Thus, locally the flow is unstratified. We might expect then, that, as for the unstratified problem, $Z_l(x)$ and $Z_u(x)$ will usually have corners at x_0. This is borne out by our numerical solutions, for which only cases with corners were found. In the light of this, the cornerless solutions obtained by Maslowe most likely result from the geometric constraints imposed, and are not an inevitable concomitant of stratification.

3.2.1. *The corner condition*

Let $Z_l(x)$ and $Z_u(x)$ meet at x_0. If $Z_l(x)$ and $Z_u(x)$ both have corners, i.e. discontinuous derivatives, at x_0, then a condition relating the vorticity in the central region to the vorticity immediately above and below the corner can be obtained.

Because $w = u\zeta_x$ it is essential that ζ_x be a continuous function of x wherever u is non-zero. Otherwise there is a discontinuity in the vertical velocity and in the pressure. In particular the vertical velocity w must be continuous along the vertical line $x = x_0$. Now w is continuous with respect to x at (x_0, Φ_0) since $u(x_0, \Phi_0) = 0$. In order that w be a continuous function of x immediately above and below this point, w_ζ must also be continuous at (x_0, Φ_0). Differentiating $w = u\zeta_x$ with respect to ζ gives

$$w_\zeta = u\frac{\partial}{\partial\Phi}(u\zeta_x) = uu_\Phi\,\zeta_x - u_x.$$

In order that w_ζ be continuous at (x_0, Φ_0) we must have

$$[u_x]_{x_0} = [uu_\Phi Z_x]_{x_0},$$

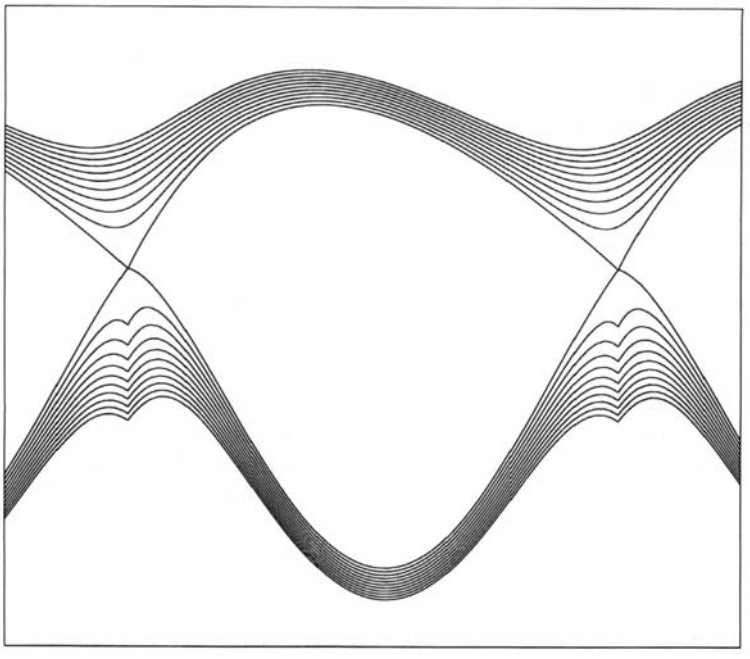

FIGURE 3. If the corner condition is not satisfied the slope of the streamlines and hence the vertical velocity have discontinuities along a vertical line on the side of the critical layer that is computed after the cat's-eyes are obtained.

where $[\,]_{x_0}$ gives the jump in value at x_0, i.e. for a general function Q,

$$[Q(x)]_{x_0} = Q(x_0^+) - Q(x_0^-).$$

Imposing this condition along $Z_l(x)$ and $Z_u(x)$ and using the fact that the vorticity is continuous along a streamline yields two equations:

$$[u_l']_{x_0} = N_l(x_0)\,[Z_l']_{x_0} = N_b[Z_l']_{x_0} \tag{3.10a}$$

and

$$[u_u']_{x_0} = N_u(x_0)\,[Z_u']_{x_0} = N_a[Z_u']_{x_0}, \tag{3.10b}$$

where N_l and N_u are the vorticities along $Z_l(x)$ and $Z_u(x)$ respectively and N_a and N_b are the values of the vorticity immediately above and below the corner.

Eliminating u_u and Z_u by using (3.6) and (3.7) results in two equations in terms of $[u_l']_{x_0}$ and $[Z_l']_{x_0}$. A non-trivial solution of these equations exists if

$$\frac{1}{N_0} = \frac{1}{2}\left(\frac{1}{N_a} + \frac{1}{N_b}\right). \tag{3.11}$$

We refer to this as the corner condition.

If this condition is not met the effects are quite dramatic. Figure 3 shows the streamlines for a case for which the corner condition is not met. In this picture the upper side was calculated first so that (3.10*b*) is satisfied but equation (3.10*a*) is not. The streamlines below the cat's-eye all have slope discontinuities along $x = x_0$ and hence discontinuities in the vertical velocity.

3.2.2. *The torque condition*

The corner condition (3.11) is a necessary condition that must be satisfied. In order to determine the three constants two more conditions are needed. A second is obtained by a consideration of the viscous stresses on the cat's-eyes. This leaves a one-parameter family of solutions, parameterized by A_u/A_l.

In the physical world viscous forces are present and so the steady inviscid solutions will be not steady but will evolve on a slow viscous timescale. We can try to minimize this drift. One approach is to consider the torque on the cat's-eyes due to viscous forces and to try to minimize it.

Applying the Rankine–Hugoniot condition to the horizontal momentum equation gives

$$-Z'(x)\,[u^2+p]+[uw-\lambda u_\zeta] = 0,$$

where [ ] is again the jump across the streamline $Z(x)$ which in this case can be either $Z_1(x)$ or $Z_u(x)$. Since u, w and p are continuous this reduces to

$$[u_z] = [uu_\phi] = 0.$$

This cannot be true for the inviscid solutions since on one side of the contour the vorticity uu_ϕ is constant, while on the other side $uu_\phi = G-\overline{Ri}Z(x)F'$ which varies with x. We can instead consider integrated values. Define M_l and M_u to be the torques per unit length along the lower and upper boundaries. Thus

$$M_{l,u} = \frac{1}{L}\int_0^L (N_{l,u}(x)-N_0)\,dx. \tag{3.12}$$

The total torque per unit length around the cat's-eyes is

$$M = \tfrac{1}{2}(M_l+M_u). \tag{3.13}$$

Defining

$$k = \overline{Ri}\,F_l'\left(Z_l(x_0)-\frac{1}{L}\int_0^L Z_l(x)\,dx\right), \tag{3.14a}$$

$$r = A_u/A_l, \tag{3.14b}$$

$$\sigma^2 = -\overline{Ri}\,A_l/L > 0, \tag{3.14c}$$

and making use of

$$N_a = G_u-\overline{Ri}\,Z_u(x_0)\,F_u', \tag{3.15a}$$

$$N_b = G_l-\overline{Ri}\,Z_l(x_0)\,F_l', \tag{3.15b}$$

gives

$$M_l = N_b-N_0+k, \tag{3.16a}$$

$$M_u = N_a-N_0-rk+\frac{2r\sigma^2}{N_0}, \tag{3.16b}$$

and

$$M = \tfrac{1}{2}(N_a+N_b)-N_0+\frac{r\sigma^2}{N_0}+\tfrac{1}{2}(1-r)k. \tag{3.16c}$$

Using the corner condition to eliminate N_b in (3.16c) gives M as a function of N_0 and the parameter r:

$$M(N_0;r) = \frac{f(N_0;r)}{N_0(2N_a-N_0)}, \tag{3.17}$$

where

$$f(N_0;r) = N_0^3-(2N_a+\tfrac{1}{2}(1-r)k)\,N_0^2+(N_a^2-r\sigma^2+(1-r)N_a k)\,N_0+2rN_a\sigma^2. \tag{3.18}$$

A requirement on the solution is that N_a, N_b and N_0 should all have the same sign, which in this case is positive. In order that $N_b > 0$ the corner condition implies that we need

$$N_0 \in (0, 2N_a). \tag{3.19}$$

Ideally we would like to have the torque equal to zero. This is not always possible. For example if $r = 1$, f becomes

$$f(N_0; 1) = N_0^3 - 2N_a N_0^2 + (N_a^2 - \sigma^2) N_0 + 2N_a \sigma^2 \tag{3.20}$$

and can easily be shown to be strictly positive on $(0, 2N_a)$. The torque condition that will be used in this paper is that N_0 is chosen to be the value of $N \in (0, 2N_a)$ which minimizes $M(N; r)$.

From now on r will be set to 1. This greatly simplifies the following analysis, which can also be done for general r. Let $g(N)$ be the total torque for the case $r = 1$. Graphs of the function $g(N)$ are given in figure 7. The independent variable $N \in (0, 2N_a)$ represents the possible values of the vorticity inside the cat's-eyes. N_0 is the value of N which minimizes g. From (3.17) and (3.18) we have

$$g(N) = \frac{f(N; 1)}{N(2N_a - N)} = \frac{N^3 - 2N_a N^2 + (N_a^2 - \sigma^2) N + 2N_a \sigma^2}{N(2N_a - N)}. \tag{3.21}$$

Since $f(N; 1) > 0$ on $(0, 2N_a)$ it follows that $g(N) \to +\infty$ as $N \to 0$ or as $N \to 2N_a$. Thus $g(N) > 0$ in $(0, 2N_a)$ and must have a minimum value in $(0, 2N_a)$. Now

$$\frac{dg}{dN} = \frac{h(N)}{N^2(2N_a - N)^2}, \tag{3.22a}$$

where

$$h(N) = -N^2(N - 3N_a)(N - N_a) - \sigma^2(N - 2N_a)^2. \tag{3.22b}$$

It is easily seen that h has one zero in $(N_a, 2N_a)$ and another zero in $(2N_a, 3N_a)$. Considering inflexion points shows that any other possible roots must lie in $(0, N_a)$. Numerical determination of N_0 is hence straightforward.

Because of the symmetry inherent in the corner condition and in $r = 1$, the above argument can be repeated by replacing N_a with N_b. All the cases described in §4 have $N_0 \in (N_a, 2N_a)$.

The above gives the procedure used to determine N_0 if $r = 1$. If $r \neq 1$ a similar analysis can be given. One possible line of pursuit would be to try and find a value of $|1 - r|$ which makes the total torque vanish, though we have not yet made any attempt to carry out this programme.

4. Continuous critical-layer solutions

In this section some global numerical solutions are presented. They all have continuous velocity and density. The vertical gradient of the basic density is assumed to be constant and to have the same value in both linear layers. Hence $A_u = A_l$ and as shown in §3 this, along with the corner condition and minimization of the total torque around the cat's-eyes, closes the problem. The sensitivity of the results to the torque condition will be discussed.

Ideally one would like to find the solutions for flow over a given hill. To do so one would have to iterate over two constants until the upper radiation condition was satisfied, because the boundary condition at the hill does not completely determine the waves in the lower linear layer. This would be a costly computational effort. A much easier procedure which yields as much interesting information about the physical characteristics of the solutions is to start with a given transmitted wave of amplitude T, find the global solution, and to then calculate a variety of hills which would give such a solution. This is the procedure followed throughout this section.

Attention is focused on the case where only a single harmonic is present in the transmitted wave, so that the forcing has the form $\Psi' = T\cos(\alpha x)$ at some height H above the critical level. This is physically realistic only if the generation of higher harmonics in the critical layer is not significant. This will be seen to be the case for a large range of parameter values.

A crude estimate of the dimensional values of the various terms, in particular the wave amplitudes and wavelength, can be obtained by the following considerations. Mean wind speeds in the atmosphere are typically of the order of 10 m s^{-1} and change by this amount over distances on the order of 1–10 km. This suggests a lengthscale of between 1000 and 10000 m. Thus, a non dimensional wave amplitude of 0.1, typical of the largest size of a transmitted wave we consider, corresponds to a dimensional height of 0.1–1.0 km, while a value of 0.00001 corresponds to an extremely small wave of 1–10 cm. With this scaling, using $\alpha = 0.1$ gives a horizontal wavelength of 60–600 km.

The remainder of this section is in four subsections. In §4.1 a few brief comments on the accuracy and interpretation of the results are made. In §4.2 a description of the general features common to all solutions is given. Section 4.3 describes in detail the effects of changing the four parameters T (transmitted wave amplitude, providing some control over the incident wave amplitude), $\overline{Ri}$ (the Richardson number of the basic flow just above the critical layer, measuring the strength of the stratification), Pr (the Prandtl number) and α (the leading horizontal wavenumber). Section 4.4 looks in more detail at some of the most physically interesting quantities, such as the reflection and transmission coefficients, hill amplitudes and resonance positions.

4.1. *Numerical accuracy*

A number of different tests were performed to check both the accuracy of the numerical method and the validity of the asymptotics. Some of the more important points are mentioned here.

In regions of steady, inviscid, x-periodic flow the Reynolds stress $\tau = \int uw\,dx$ is constant with height. This provides a useful criterion for determining whether a valid global solution has been obtained. For most of the solutions presented in this and the following sections the Reynolds stress in the two linear layers differed by about 10^{-3}%. For parameter values near certain critical values this error rises extremely rapidly. A solution is deemed valid if the two Reynolds stresses differ by less than about 0.5%. This value is arbitrary and not crucial because for solutions with such an error, changing the parameter values by 1% (in the appropriate direction) increases this error by a factor of 10 or more.

As will be seen in§4.3 the accurate determination of N_a, the vorticity immediately above the cat's-eye corner, is vital. This requires an accurate solution of the ordinary differential equations in the critical layer. The equations are singular at the cat's-eye corner where the horizontal velocity is zero. Because of this they can only be solved up to a streamline along which the velocity becomes very small but is still non-zero. How close the streamline on which u first becomes zero can be approached depends on the number of grid points P, the accuracy requirements and the minimum step size $h_{\min}$ allowed by the ordinary differential equation integrators. Both a fourth-order adaptive step Rune–Kutta method and a Bulirsch–Stoer method were tried, giving the same results. Using 1024 grid points in the horizontal direction and a minimum step size of about 1.0×10^{-9} gave sufficiently accurate results.

It was found that the numerical results can be very sensitive to the choice of the contour at which the upper linear solution is numerically matched to the inner

nonlinear solution. This sensitivity is a numerical artifact. For example, using $\tanh(z)$ as the mean velocity, matching at $z = 0.2$ or $z = 0.4$ gave radically different solutions for the simple reason that $z = 0.4$ is not small enough for the asymptotic approximation $\bar{U} \approx z$ to be valid. Thus the vorticity of the mean flow is very different at the two values of z. Maslowe's viscous secularity condition (which is enforced only in the nonlinear region, however one should choose to define its boundaries) essentially drives the flow to constant density and velocity gradients, with values set by values at the matching contour. For the numerical calculations one must be careful that the matching contour has values of z sufficiently small so that $\bar{U} \approx z$.

In some sense, this unphysical sensitivity represents a failure of the asymptotics, as the external forcing terms which would maintain the large-scale flow against diffusion are asymptotically negligible in (2.17) and (2.18); yet the timescale for diffusing out the large-scale background flow is so long that the effect of the forcing terms would become important. An alternative interpretation is that during the evolution to a final steady state the mean flow is significantly modified well beyond the boundaries of the nonlinear critical layer of the final state, i.e. the nonlinear layer is thicker during its evolution than during its final steady state.

The use of a mean flow which has constant vorticity in a large neighbourhood of the critical layer allows us to sidestep this numerical difficulty. The mean flow used for all the results cited here is

$$\bar{U}(z) = \begin{cases} 1.0 & (z > 1.5) \\ p(z) & (0.6 \leqslant x \leqslant 1.5) \\ z & (z < 0.6), \end{cases} \tag{4.1}$$

where $p(z)$ is a fifth-degree polynomial whose coefficients are chosen so that $\bar{U}$ and its first two derivatives are continuous. Because the ordinary differential equation for the vertical structure in the linear region involves the second derivative of $\bar{U}$ it is necessary to make $\bar{U}'$ and $\bar{U}''$ continuous. Otherwise there would be extraneous reflections at their discontinuities. The important feature of this basic profile is that it has a vorticity which is equal to 1.0 in a wide neighbourhood of $z = 0$. Any other basic profile with this feature would do.

On the other side of the critical layer the match to the lower linear layer is done at constant z (the numerical procedure for this is discussed below). A basic velocity profile for the lower linear layer must be chosen in such a way that the velocity and its first two derivatives are continuous at the matching level. It is also chosen so that it asymptotes to some constant value far from the critical level. The constant value will always be taken to be -1.0. If the match to the linear layer were performed at a z level where the mean velocity is close to -1.0, the mean velocity profile would have a large overshoot and regions of large curvature, leading to unwanted partial reflections. In order to minimize this effect an attempt was made to start the lower linear layer well before the mean velocity reached -1.0. This was not always possible because if the waves are large enough the flow does not become linear until the mean horizontal velocity is comparable to -1.0. We have chosen to restrict attention to amplitude ranges for which the nonlinear region retains its character as a thin critical layer with scale distinctly smaller than that of the background shear flow.

In order to monitor the influence of the basic velocity profile all cases were run with two different velocity profiles. The first has the form

$$\bar{U}(z) = \tanh(a(z - z_0)) + C\,\mathrm{e}^{z}, \tag{4.2}$$

where the constants a, c and z_0 were chosen in order to make $\bar{U}$, $\bar{U}'$ and $\bar{U}''$ continuous

at the matching level. Note that $U(z)+1 \to 0$ exponentially as $z \to -\infty$. The second velocity profile used was of the form

$$\bar{U}(z) = \begin{cases} f(z) & (z_p \leqslant z \leqslant z_m) \\ -1.0 & (z < z_p), \end{cases} \tag{4.3}$$

where z_m is the matching level, $f(z)$ is a fifth-degree polynomial chosen so that $\bar{U}, \bar{U}'$ and $\bar{U}''$ are continuous. The choice of z_p varies so that the bump in this velocity profile is not too large. Typically the exponential fit (4.2) yields a velocity profile with a much smaller overshoot than does the polynomial profile (4.3). Comparing the results for two velocity profiles allows one to judge the importance of the choice of the velocity profile. In particular, when studying the effects of changing the various parameters on the size of the reflected and incident waves we can determine how much of the effect is due to the change in the mean velocity profile in the lower linear layer. Throughout the remainder of this section all the results cited are those for the exponential fit given by (4.2). The conclusions based on the second profile are the same as for the exponential profile. The reflected and incident waves were generally larger but the critical parameter values for which a solution could no longer be obtained are not significantly changed.

Numerically, the transition from the critical-layer equations to the linear equations must be done at a particular value $z = z_m$. From the critical-layer solution one calculates $\Psi(x, z_m)$, $\Psi_z(x, z_m)$, $\Psi_{zz}(x, z_m)$, $\Psi_{zzz}(x, z_m)$, $\rho(x, z_m)$ and $\rho_z(x, z_m)$. These are then decomposed into Fourier series comprising a mean value and a perturbation with zero mean. In the linear layer the solution has the form

$$\Psi(x, z) = \bar{\Psi}(z) + \epsilon\tilde{\Psi}(x, z), \quad \rho(x, z) = \bar{\rho}(z) + \epsilon\tilde{\rho}(x, z). \tag{4.4}$$

The Fourier decomposition of the nonlinear solution at z_m is used to initialize the linear solution. All harmonics are retained.

Verification that z_m does indeed lie in the matching region can be done as follows. In the linear layer, $\tilde{\Psi}$ and $\tilde{\rho}$ are governed by equations which give a relationship between $\tilde{\Psi}_{zz}$ and $\tilde{\Psi}$ as well as between $\tilde{\Psi}$ and $\tilde{\rho}$ (see (2.6)). These relationships should hold for the perturbations in the critical layer at the matching level, and checking these shows that the agreement is very good for the leading harmonic. The agreement is very bad for the higher harmonics if they have an amplitude which is much smaller than those of the leading harmonics. The source of the difficulty is that, if the ratio of the amplitudes of the higher harmonics to that of the first harmonic is of the same size as ϵ, then the nonlinear contributions to the flow from the first harmonics can be just as important as the linear contributions of the higher harmonics. Because of this, if the higher harmonics are small compared to the leading harmonic we cannot draw any conclusions about the higher harmonics except for their size relative to the leading harmonic.

4.2. *General description of the global solution*

Before discussing the effects of varying the values of the parameters some of the features common to all solutions are presented in this section.

The constancy of the Reynolds stress with height has an important consequence for the global behaviour. It implies that wave global over-reflection occurs at the critical layer whenever there is a non-vanishing transmitted wave. In particular, below the critical layer the total momentum flux in the downward-propagating waves must be larger than the momentum flux in the waves propagating upwards.

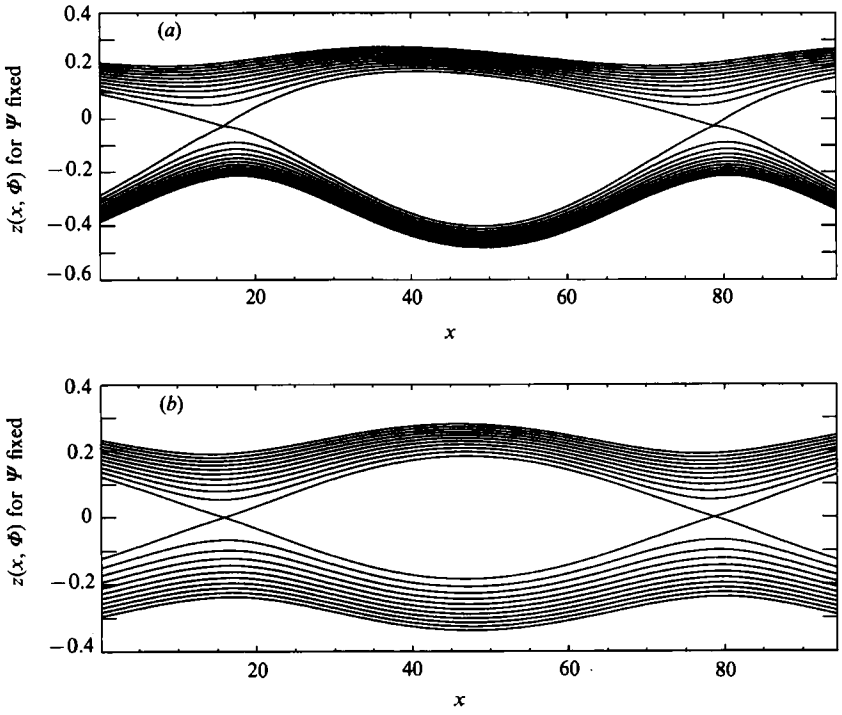

FIGURE 4. (*a*) A series of streamlines in the critical layer. The contours are plotted at constant intervals in the stream function. (*b*) Plots of the horizontal velocity as a function of x for the same values of the stream function. The parameter values are $(\overline{Ri}, T, Pr, \alpha) = (0.4, 0.02, 1.1, 0.1)$.

For at least one mode then, the reflected wave must be larger than the incident wave. This should apply to the leading harmonics if they dominate. Generally this is the case, except for extreme cases near critical parameter values where most of the momentum flux is in the second harmonic.

The reflected and incident waves are also usually much larger than the transmitted wave. This means that the flow in the lower linear layer can be nonlinear even for fairly small transmitted waves owing to the combined response of the reflected and incident waves at certain heights. For this reason most of the results cited are for small values of T; they are characterized by nearly perfect reflection, with relatively little transmission.

In all cases computed N_a, the vorticity immediately above the corner of the cat's-eyes, was smaller than N_b, the value of the vorticity immediately below. N_a was always significantly less than 1.0, usually in the range 0.2–0.7. The vorticity N_0 inside the cat's-eyes was always in $(N_a, 2N_a)$ and was less than 1.0. This is an important point because the thickness of the cat's-eyes is inversely proportional to N_0. Thus the shape of the lower cat's-eye boundary, and hence the size of the incident and reflected wave, is largely determined by the value of N_0.

A typical critical-layer structure is shown in figure 4. Figure 4(*a*) shows a series of streamlines (i.e. $z(x, \Phi)$ for different values of Φ). The graphs are depicted using the outer vertical coordinate z so that the horizontal and vertical scales are the same. Figure 4(*b*) shows the horizontal velocities (using rescaled critical layer velocity) along the same streamlines. Note the asymmetry in the streamlines between the upper and lower boundaries of the cat's-eyes. The upper boundary has its maximum to the left of the centre of the cat's-eyes while the lower boundary has its minimum

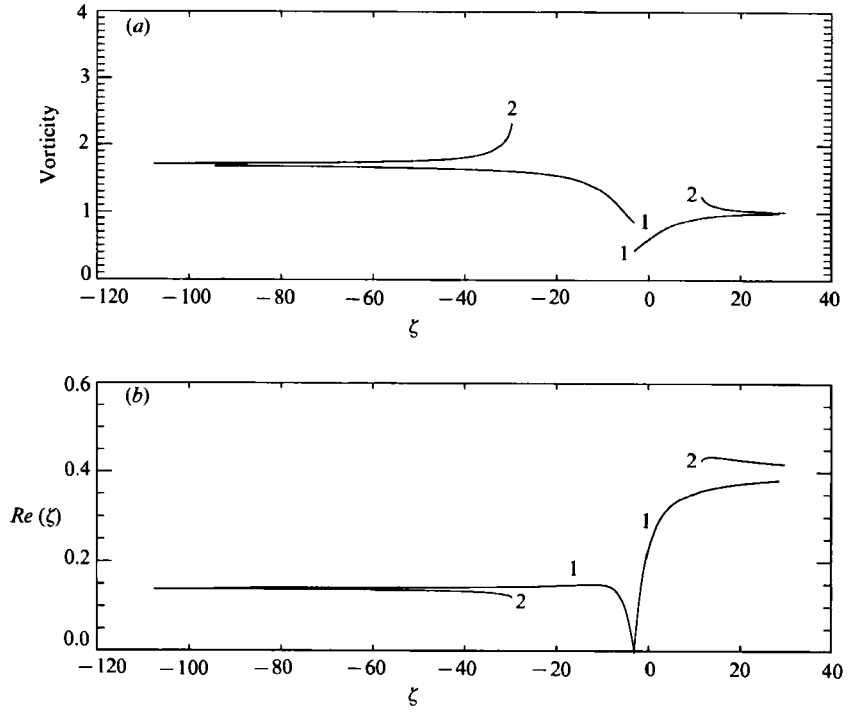

FIGURE 5. (*a*) The total vorticity and (*b*) the total Richardson number Ri along vertical lines through the critical layer. One line (labelled 1) passes through the cat's-eye corner where Ri becomes zero. The other (line 2) is midway between two cat's-eye corners and does not include the interior of the cat's-eyes. Both quantities approach constant values as one moves away from the cat's-eyes. $(\overline{Ri}, T, Pr, \alpha) = (0.4, 0.02, 1.1, 0.1)$.

to the right of the centre. Notice also the apparent phase shift, in contrast with the behaviour (for trapped modes) found by Stewartson (1981) (see also Maslowe 1986). A similar asymmetry is not possible for the horizontal velocity since the velocities along the upper and lower boundaries are related by $u_l(x) = -u_u(x)$. Figure 4 also indicates another property of all solutions calculated: significant enhancement of the vorticity in conjunction with a large decrease in the total Richardson number $Ri\,(=\overline{Ri}\,uF'/u_\zeta^2)$. Away from the cat's-eye boundaries the vorticity and the total Richardson number have fairly constant values. This is indicated in figure 5, which shows how the vorticity (figure 5*a*) and Ri vary as functions of ζ along two vertical lines in the critical layer, one passing through the cat's-eye corner and one midway between two corners. Note that the vorticity and Ri rapidly approach constant values as one moves away from the cat's-eye boundary. This is because the vorticity is equal to $G-\overline{Ri}\,\zeta F'$. As $\Phi\to\infty, F'\to 0$ and the vorticity approaches G which is independent of x and asymptotes to a constant.

It is interesting to note that the total Richardson number Ri is always found to be less than 0.25 in a thin layer along the lower side of the critical layer, typically having values in the range 0.05–0.15. The Miles–Howard theorem thus implies that these solutions might be unstable to Kelvin–Helmholtz instabilities. Because the theorem provides only a necessary condition for instability, a numerical stability analysis would be necessary to settle the question.

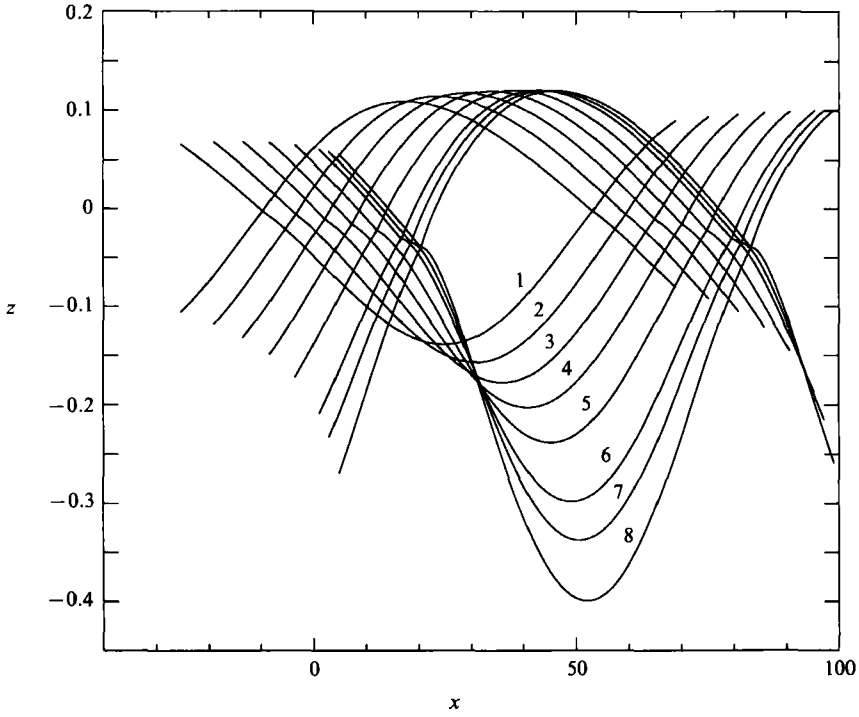

FIGURE 6. Cat's-eyes for different values of the Richardson number $\overline{Ri}$. Increasing $\overline{Ri}$ deepens the lower cat's-eye boundary. The parameter values are $(T, Pr, \alpha) = (0.01, 1.1, 0.1)$. Curve 1, $\overline{Ri} = 0.15$; 2, 0.20; 3, 0.25; 4, 0.30; 5, 0.35; 6, 0.40; 7, 0.42; 8, 0.44.

$\overline{Ri}$	N_a	N_0	N_b	R_1	I_1	N_m	Ri_m
0.20	0.781	0.867	0.976	0.01507	0.01127	1.221	0.134
0.25	0.713	0.817	0.958	0.01758	0.01445	1.228	0.150
0.30	0.635	0.756	0.934	0.02138	0.01890	1.370	0.159
0.35	0.545	0.679	0.900	0.02785	0.02602	1.487	0.158
0.40	0.435	0.576	0.856	0.04205	0.04095	1.692	0.139
0.42	0.381	0.523	0.833	0.05385	0.05313	1.835	0.124
0.44	0.319	0.457	0.805	0.07473	0.07461	2.068	0.102
0.46	0.244	0.437	0.773	0.11493	0.11669	2.522	0.072
0.48	0.148	0.247	0.735	—	—	—	—

TABLE 1. Effect of varying $\overline{Ri}$ for $(T, Pr, \alpha) = (0.01, 1.1, 0.1)$

4.3. *Dependence on T, $\overline{Ri}$, Pr and α*

Consider first the effects of varying $\overline{Ri}$. Some pertinent values for the case $T = 0.01$, $Pr = 1.1$ and $\alpha = 0.1$ are given in table 1. The quantities R_1 and I_1 are the amplitudes of the first harmonics of the reflected and incident waves respectively. The term N_m and Ri_m are the mean values of the vorticity and total Richardson numbers at z_m, the level used to match the critical layer to the lower linear layer. At this level the variation of the vorticity and the Richardson number is small compared with their mean values. Dashes indicate that a global solution was not obtained.

As $\overline{Ri}$ is increased the value of the vorticity immediately above the cat's-eye corners, N_a, decreases and approaches zero. This is the most important trend because

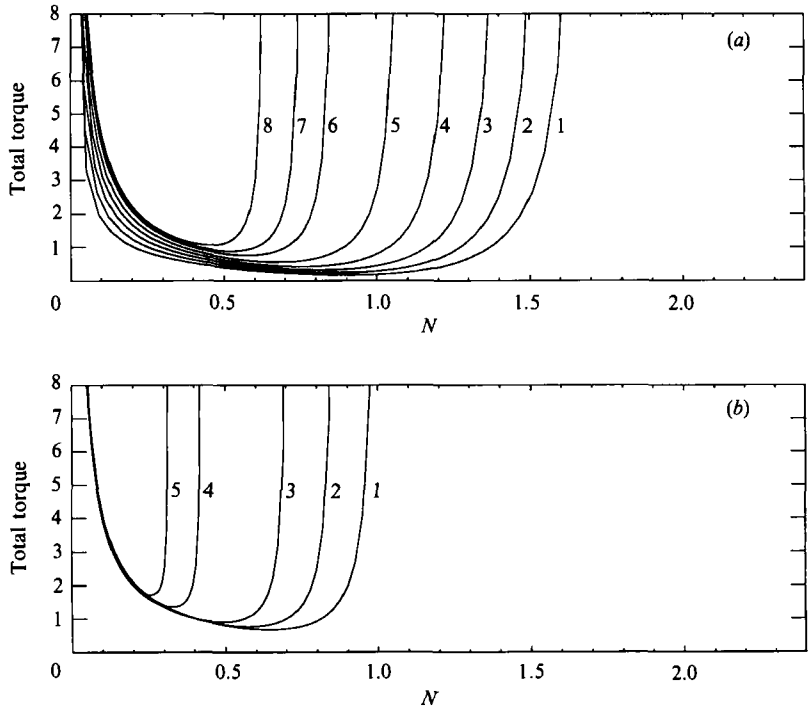

FIGURE 7. The total torque around the cat's-eyes plotted as a function of N, the vorticity inside the cat's-eyes. N has values between 0 and $2N_a$. As N_a decreases, the value N_0 which minimizes the torque approaches its maximum possible value of $2N_a$. The minimum also becomes more pronounced. For both graphs $Pr = 1.1$ and $\alpha = 0.1$. (*a*) $T = 0.01$, and curve 1, $\overline{Ri} = 0.15$; 2, 0.20; 3, 0.25; 4, 0.30; 5, 0.35; 6, 0.40; 7, 0.42; 8, 0.44. (*b*) $\overline{Ri} = 0.4$, and curve 1, $T = 0.02$; 2, 0.01; 3, 0.005; 4, 0.002; 5, 0.0016.

the value of N_a is a very important indicator of whether or not there is a global solution. The vorticity in the centre, N_0, also decreases (as expected since it is bounded by $2N_a$) so that the cat's-eyes become thicker. The shape of the upper boundary does not change very significantly. It is the lower contour which greatly increases its vertical span owing to the decreasing value of N_0. This implies that the waves on the lower side of the critical layer become larger as $\overline{Ri}$ increases, and the critical level becomes a more nearly perfect reflector. Figure 6 shows a series of cat's-eyes for $T = 0.01$ clearly illustrating this trend.

The reason for the decrease in N_a is the following. The perturbation vorticity in the linear layer is given by

$$\tilde{\Psi}_{zz} = \left(\frac{\overline{Ri}}{\bar{U}^2}\rho' + \frac{\bar{U}''}{\bar{U}} + \alpha^2\right)\tilde{\Psi}.$$

In the matching region, where $\bar{U}$ is small, the first term in the coefficient of $\tilde{\Psi}$ is negative and dominates the other two terms. Increasing $\overline{Ri}$ thus increases the variation in $\tilde{\Psi}_{zz}$, making its minimum value smaller for a given mean value. This minimum value occurs where $\tilde{\Psi}$ has its maximum; in the trough (crest) of a streamline if $u > 0$ ($u < 0$) (i.e. above (below) the cat's-eyes). The solution in the critical layer maintains this pattern so that the minimum value of the vorticity along the upper boundary of the cat's-eyes occurs very close to the corner. In connection with this, changing $\overline{Ri}$ has very little effect on the mean vorticity in the upper critical layer as illustrated in figure 8(*b*).

The ratio N_0/N_a increases from about 1.11 for $\overline{Ri} = 0.2$ to 1.32 for $\overline{Ri} = 0.4$ and up to 1.79 for $\overline{Ri} = 0.46$. Thus, as the solution is about to break down the torque condition attempts to make the vorticity in the cat's-eyes as large as possible and hence to make the cat's-eyes as thin as possible. This trend can be seen in figure 7 (*a*) which shows, for different values of $\overline{Ri}$, plots of the total torque as a function of the possible values of N_0. Note that not only does the value N_0 of the cat's-eye vorticity which minimizes the torque approach its maximum possible value, but the minimum of the total torque also becomes more pronounced and increases.

Once N_a becomes too small (≈ 0.2) the solution breaks down. The breakdown is expected since as $N_a \to 0$ the cat's-eyes are forced to become infinitely thick. The solution (at any resolution) develops two corners at the grid points to either side of the cat's-eye corner. This behaviour seems to be tied in to the fact that the vorticity becomes slightly negative on one side of the corner. The two corners, situated where $u \neq 0$, are physically unacceptable. This behaviour is observed to happen after the solution has reached a regime for which the waves below the critical layer are very large and increasing rapidly with $\overline{Ri}$.

Two other interesting features of the solutions are that N_m is always significantly greater than 1.0, the vorticity above the cat's-eyes, and Ri_m is always significantly less than 0.25. As $\overline{Ri}$ increases the mean vorticity N_m increases. This trend is due to the function G below the lower cat's-eye boundary which increases dramatically as one moves away from the boundary. Its final value far from the cat's-eye increases with $\overline{Ri}$ even though its initial value at the lower cat's-eye boundary decreases. Figure 8 shows how G and the mean vorticity vary with $\overline{Ri}$.

To understand the increase in vorticity consider its mean value along the lower cat's-eye boundary, which can be written as

$$N_b + \overline{Ri}\, F'_b \left(\zeta_0 - \frac{1}{L} \int_0^L Z_1(x)\, dx \right).$$

ζ_0 is the value of ζ at the cat's-eye corner and F'_b is the positive value of F' along the lower cat's-eye boundary, which is essentially $\overline{Ri}$. Owing to the deepening of the lower cat's-eye boundary, ζ_0 minus the mean value of ζ along the boundary increases. The resulting large growth of the second term offsets the small decrease in N_b. Note that below the cat's-eyes the vorticity along a streamline has its minimum value at the top of the streamline. Accompanying the significant increase of vorticity is a significant drop in the total Richardson number once $\overline{Ri} > 0.35$, after which the large increase in vorticity more than compensates the increase in $\overline{Ri}$.

For very large values of $\overline{Ri}$ a different picture emerges. The vorticity changes sign before the horizontal velocity becomes zero so that the horizontal velocity starts to increase before it becomes zero. No cat's-eyes are obtained. The calculation shows that a very different regime sets in for initial states with large $\overline{Ri}$. In this regime the steady state is not characterized by a small shift of the critical layer from that of the ambient flow; instead, for an initial state with a large Richardson number, one may expect large mean flow modifications so that the Richardson number of the mean flow is significantly reduced before a steady state is achieved. This scenario does not contradict the solutions obtained by Brown & Stewartson (1982) who studied the initial-value problem for large Richardson numbers. Their solutions are valid only for a finite length of time and do not say anything about the solution after an infinite amount of time.

In summary, increasing $\overline{Ri}$ decreases the minimum value of the vorticity along the streamline used to match the upper linear layer to the critical layer. This decrease is

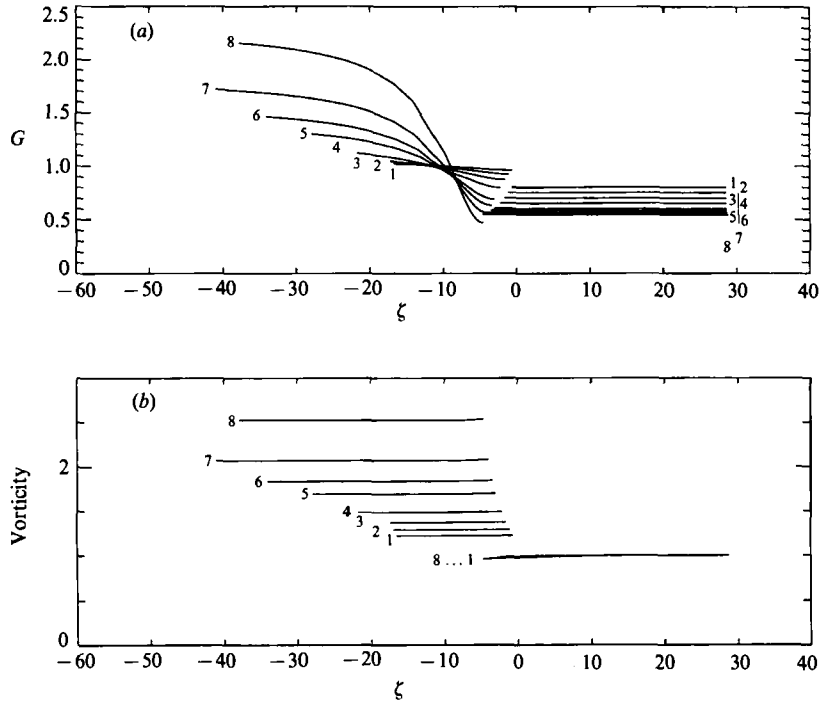

FIGURE 8. Profiles of (*a*) G and (*b*) the mean vorticity (average value along a streamline) for different values of $\overline{Ri}$ plotted as functions of ζ along a vertical line passing through the corner so that the functions above and below the cat's-eyes are separated (T, Pr, α) = (0.01, 1.1, 0.1). Curve 1, $\overline{Ri}$ = 0.20; 2, 0.25; 3, 0.30; 4, 0.35; 5, 0.40; 6, 0.42; 7, 0.44; 8, 0.46.

T	N_a	N_0	R_1	I_1	N_m	Ri_m
0.075	0.605	0.748	0.1923	0.1750	1.69	0.142
0.050	0.578	0.722	0.1359	0.1256	1.67	0.144
0.040	0.561	0.705	0.1125	0.1047	1.67	0.145
0.030	0.538	0.681	0.0893	0.0839	1.67	0.145
0.020	0.501	0.644	0.0659	0.0628	1.67	0.145
0.010	0.435	0.576	0.0421	0.0410	1.71	0.139
0.0075	0.403	0.544	0.0363	0.0357	1.74	0.134
0.005	0.356	0.493	0.0312	0.0309	1.81	0.124
0.004	0.326	0.460	0.0297	0.0296	1.87	0.115
0.003	0.285	0.414	0.02936	0.02941	2.00	0.101
0.002	0.212	0.327	0.03546	0.03582	2.40	0.070

TABLE 2. Effect of varying T for ($\overline{Ri}$, Pr, α) = (0.4, 1.1, 0.1)

reflected in a decrease in N_a which in turn results in a smaller vorticity inside the cat's-eyes and to a deepening of the lower cat's-eye boundary. Larger incident and reflected waves are the result so that the critical layer becomes a more nearly perfect reflector. Accompanying this is a vorticity greater than 1.0 and a total Richardson number less than 0.25 below the critical layer. If $\overline{Ri}$ is too large the solution breaks down because N_a gets too close to zero. For still larger values the vorticity becomes negative before the flow goes to zero and an upper cat's-eye boundary is never attained, indicating no steady states in this regime.

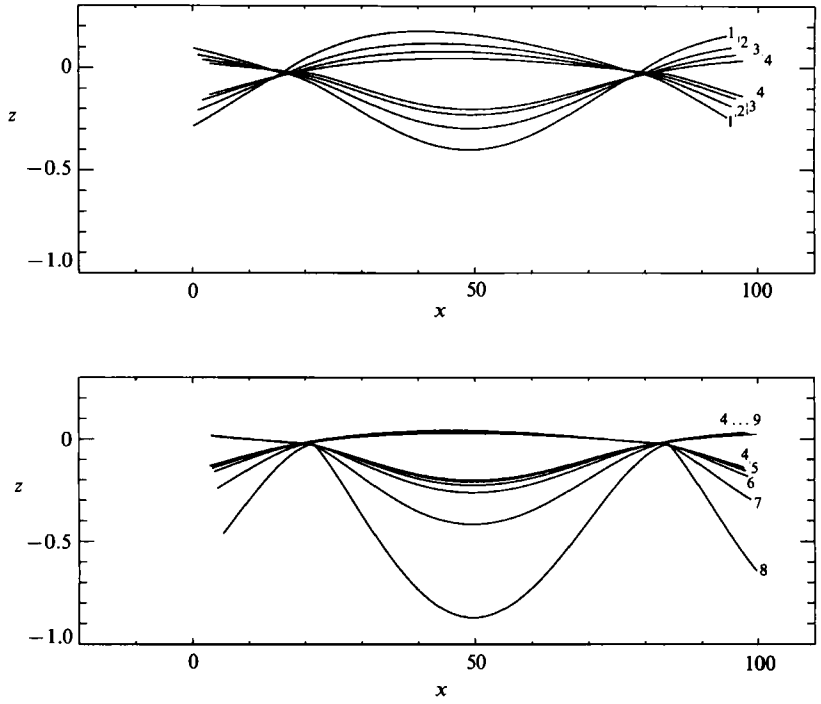

FIGURE 9. Cat's-eyes for different amplitudes T of the transmitted wave. As T decreases, the cat's-eyes become thinner at first but then start to thicken very rapidly as T decreases further. This thickening is due to the decreasing value of N_0 and the resulting deepening of the lower boundary. The upper boundary continues to decrease in amplitude. $(\overline{Ri}, Pr, \alpha) = (0.4, 1.1, 0.1)$. Curve 1, $T = 0.020$; 2, 0.010; 3, 0.005; 4, 0.002; 5, 0.0018; 6, 0.0016; 7, 0.0014; 8, 0.0012; 9, 0.0010.

Consider now the effect of varying T, the amplitude of the transmitted wave. Table 2 gives some values for the case $\overline{Ri} = 0.4$, $Pr = 1.1$ and $\alpha = 0.1$. As T is decreased N_a decreases, leading to a breakdown of the solution just as for the case of increasing $\overline{Ri}$. Figure 9 shows a sequence of the cat's-eye boundaries for varying T. Figure 9(a) shows four of the cases given in the table: $T = 0.020$, 0.010, 0.005 and 0.002. Figure 9(b) covers the cases $T = 0.001$ to 0.002 in steps of 0.0002. Even though N_0 is decreasing the cat's-eyes decrease in thickness for a while. The thickness is proportional to u_u/N_0 and the decrease in u_u, the horizontal velocity along the upper boundary, dominates the decrease in N_0. For N_0 sufficiently small its decrease dominates and the cat's-eyes start to get thicker. The two graphs in figure 9 illustrate that the cat's-eyes have a minimum thickness, in this case at about $T = 0.002$, and that the transition from decreasing to increasing thickness is continuous. The solution breaks down at about $T = 0.0016$ where $N_a = 0.159$. Note that as in the case of increasing $\overline{Ri}$ the solution breaks down when N_a is less than about 0.2. Figure 7(b) shows the total torque for different values of T. As for the case of varying $\overline{Ri}$, as N_a decreases the minimum value of the total torque increases, the minimum becomes more pronounced and the value of $N_0/2N_a$ approaches 1.

Below the cat's-eyes the vorticity is again much larger than 1.0 and the total Richardson number is much less than 0.25. As the wave amplitude decreases, the vorticity below the cat's-eyes is fairly constant until T is less than about 0.01 when the vorticity starts to rise.

As for the case of increasing $\overline{Ri}$ all the trends shown in table 2 are governed by the decrease in the value of N_a. The vorticity N_a just above the cat's-eye corner is given

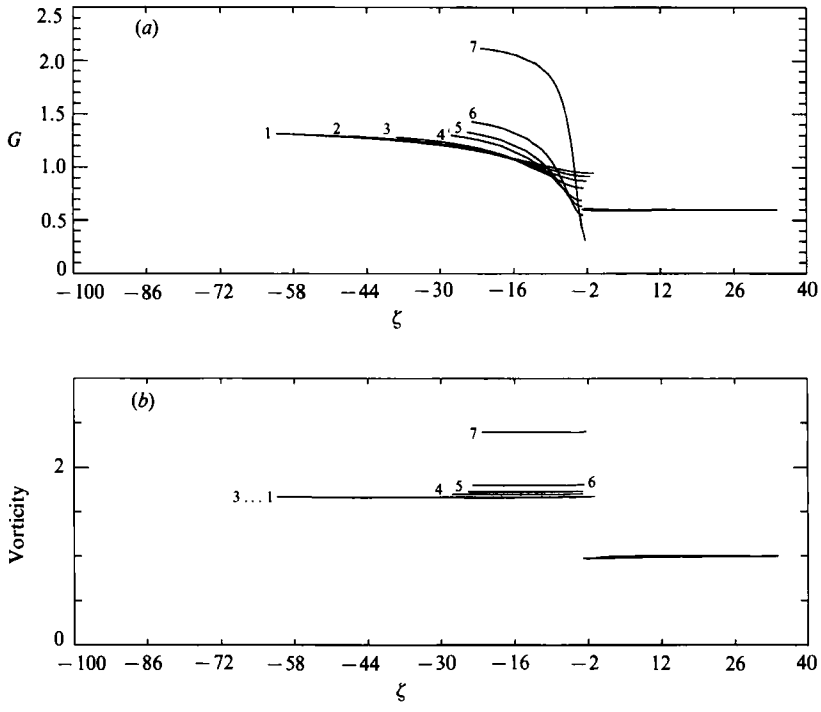

FIGURE 10. Profiles of (*a*) G and (*b*) the mean vorticity (average value along a streamline) for different values of T vorticity plotted as functions of ζ along a vertical line passing through the corner so that the functions above and below the cat's-eyes are separated. $(\overline{Ri}, Pr, \alpha) = (0.4, 1.1, 0.1)$. Curve 1, $T = 0.05$; 2, 0.04; 3, 0.03; 4, 0.02; 5, 0.01; 6, 0.005, 7, 0.002.

T	G_a	F'_a	ζ_0	$\zeta_0 F'_a$
0.075	0.5896	−0.0394	0.9708	−0.038
0.050	0.5927	−0.0503	−0.7156	0.036
0.040	0.5942	−0.0575	−1.432	0.082
0.030	0.5960	−0.0686	−2.126	0.146
0.020	0.5984	−0.0882	−2.759	0.243
0.010	0.6026	−0.1373	−3.060	0.420
0.0075	0.6044	−0.1659	−3.031	0.503
0.005	0.6071	−0.2179	−2.883	0.628
0.004	0.6087	−0.2539	−2.783	0.707
0.003	0.6108	−0.3106	−2.621	0.814
0.002	0.6141	−0.4163	−2.415	1.005

TABLE 3. Effect of varying T on G_a, F'_a and ζ_0 $(\overline{Ri}, Pr, \alpha) = (0.4, 1.1, 0.1)$

by $N_a = G_a - \overline{Ri}\,\zeta_0 F'_a$, where ζ_0 is the value of ζ at the corner and G_a and F'_a are the values of G and F' along the upper cat's-eye boundary. Figure 10 shows how G and the mean vorticity vary with T for $Pr = 1.1$. Above the cat's-eyes G is essentially independent of T. Thus the change in N_a is due to changes in $\zeta_0 F'_a$ which increases as T decreases. Table 3 shows that the decrease in N_a is due to the large increase in F'_a. The reason for this large increase is quite simple. Recall that the equation for F is

$$F' = A \Big/ \int_0^L u\,\mathrm{d}x,$$

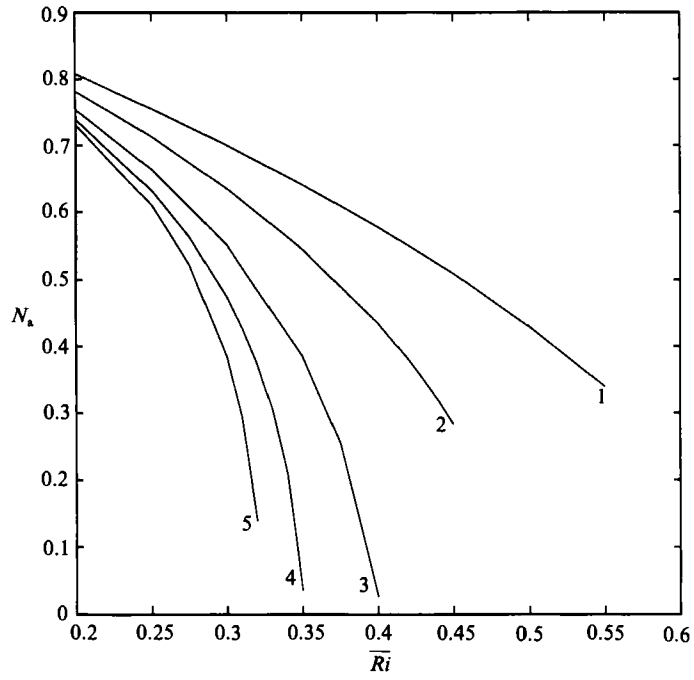

FIGURE 11. The vorticity immediately above the cat's-eye corner, N_a, as a function of $\overline{Ri}$ plotted for different values of T. $(Pr, \alpha) = (1.1, 0.1)$. Curve 1, $T = 0.05$; 2, 0.01; 3, 0.001; 4, 0.0001, 5, 0.00001.

where $A = L\overline{\rho}_c'$ is a constant independent of T. As $T \to 0$ the variation in u along the upper cat's-eye boundary decreases and, because its minimum value is always zero, its mean value decreases as well. Hence F_a' increases in magnitude.

We would also expect that as the wave amplitude decreases, ζ_0 would approach zero, possibly offsetting the increase in F_a'. For the cases calculated, ζ_0 actually moves away from 0 as T decreases as long as T is greater than a certain size. Decreasing T below this threshold starts to move ζ_0 toward zero, but not quickly enough to compensate for the large growth of F_a'.

The above argument suggests that the particular form of F' determined by the viscous secularity condition plays an important role in the outcome. The particular form of F' used here guarantees that the value of the vertical density gradient averaged along a contour remains constant, equal to $\overline{\rho}_c'$. Any functional form for F which somehow guarantees that the mean value of ρ_ξ stays below some negative value will guarantee that F' increases as $T \to 0$. How this balances with changes in ζ_0 would depend on the particular form of F.

Increasing $\overline{Ri}$ and decreasing T both decrease the value of the vorticity immediately above the cat's-eye corner. In both cases the solution breaks down when N_a becomes less than about 0.2. As $\overline{Ri}$ is increased the minimum value of T required for a solution increases. This suggests that there is a certain inescapable (but still rather small) amount of transmission, which increases with increasing stratification.

Some of the effects of varying both $\overline{Ri}$ and T are shown in figures 11–13. Figure 11 shows a series of plots of N_a *vs.* $\overline{Ri}$ for different amplitudes of the transmitted wave. It clearly shows that increasing T increases the maximum value of $\overline{Ri}$ for which there is a solution and that increasing $\overline{Ri}$ increases the lower bound on the size of the

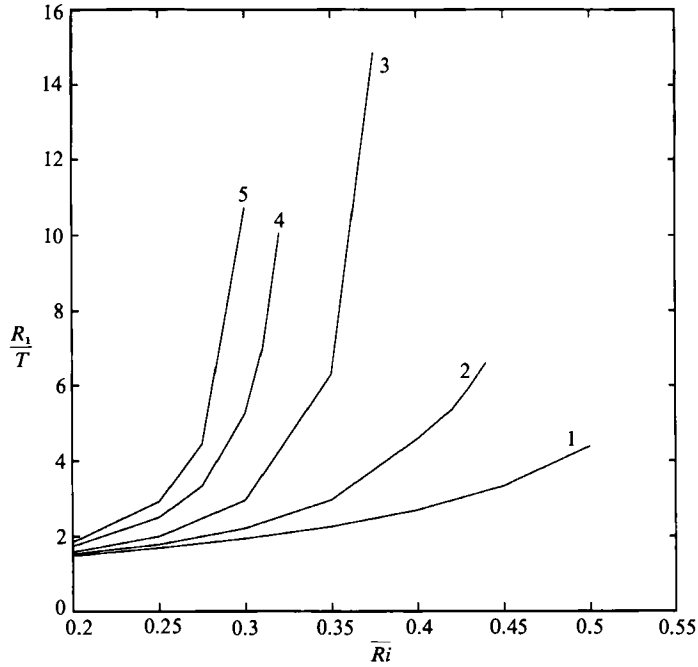

FIGURE 12. The ratio of R, the amplitude of the reflected wave (leading harmonic), to the amplitude of the transmitted wave T as a function of the Richardson number $\overline{Ri}$ plotted for different values of T. $(Pr, \alpha) = (1.1, 0.1)$. Curves 1–5 as figure 11.

transmitted wave. For example, for $\overline{Ri} = 0.5$ the amplitude T must be greater than 0.01 in order for there to be a solution (i.e. for N_a to be greater than 0.2). Plotting cat's-eyes for varying T for this value of $\overline{Ri}$ would result in a pattern similar to that shown in figure 9, with the minimum thickness and breakdown of the solution both occurring for larger values of T than for those for $R = 0.4$. For a smaller value, say $\overline{Ri} = 0.3$, the solution is still valid for $T = 0.000\,01$ and in order to get a minimum thickness and a breakdown of the solution the value of T would have to be much smaller. Figure 12 shows how the ratio R_1/T varies with $\overline{Ri}$ for different values of T. It shows that R_1/T increases as $\overline{Ri}$ increases with T fixed and that it increases as T decreases with $\overline{Ri}$ fixed. Finally figure 13 shows how the ratio R_1/T varies with T for different values of $\overline{Ri}$. For large transmitted waves the ratio of the reflected and transmitted waves is largely independent of T. As $\overline{Ri}$ gets smaller the ratio approaches 1, the value for an unstratified fluid ($\overline{Ri} = 0$).

The overall picture is that weakly stratified nonlinear critical layers are very permeable to gravity waves, but even a moderate amount of stratification (about enough to make the ambient flow stable by the Miles–Howard criterion) turns them into rather good reflectors. Other things being equal, low-amplitude waves are transmitted less than high-amplitude waves, with the amplitude sensitivity becoming more pronounced with increasing stratification.

The effect of varying the Prandtl number Pr is now considered. The only way that the Prandtl number enters the problem is as a parameter in the equation for G (equation (2.18)). Considering various values of Pr is equivalent to considering a one-parameter family of functions G. Because Pr appears in the forms $1/Pr$ and $(1-Pr)/Pr$ the effect of varying Pr is quite small if Pr is much larger than 1.0. Table 4 gives some pertinent values for a series of cases for which $\overline{Ri} = 0.4$, $T = 0.02$ and

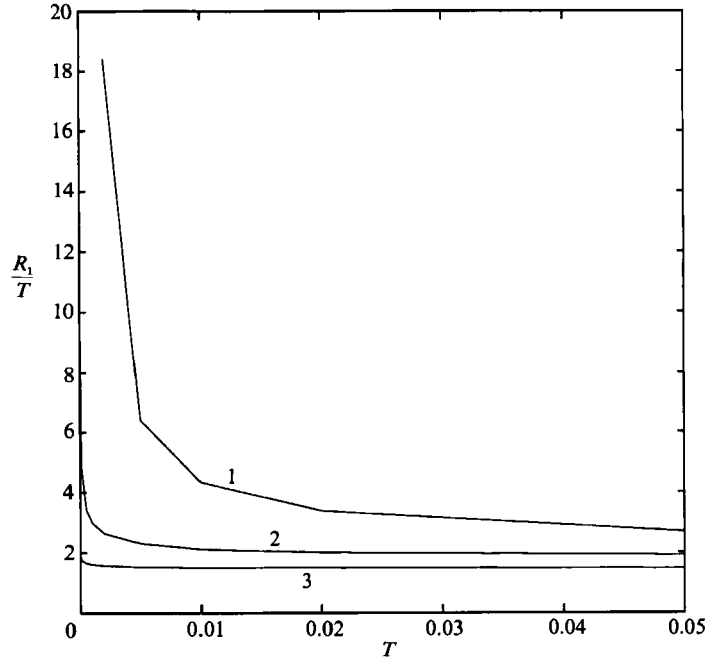

FIGURE 13. The ratio of R, the amplitude of the reflected wave (leading harmonic), to the amplitude of the transmitted wave T as a function of T plotted for different values of $\overline{Ri}$. $(Pr, \alpha) = (1.1, 0.1)$. Curve 1, $\overline{Ri} = 0.3$; 2, 0.2; 3, 0.1.

Pr	N_a	N_0	R_1	I_1	N_m	Ri_m
0.25	0.673	0.815	0.03564	0.02971	1.33	0.22
0.50	0.565	0.709	0.05118	0.04720	1.50	0.18
0.75	0.527	0.671	0.05928	0.05585	1.59	0.16
1.00	0.507	0.650	0.06446	0.06130	1.64	0.15
1.50	0.486	0.629	0.07039	0.06747	1.70	0.14
2.00	0.476	0.619	0.07360	0.07080	1.73	0.13
4.00	0.460	0.603	0.07908	0.07645	1.79	0.13
8.00	0.452	0.594	0.08228	0.07974	1.81	0.12

TABLE 4. Effect of varying Pr for $(\overline{Ri}, T, \alpha) = (0.4, 0.02, 0.1)$

$\alpha = 0.1$. The most important trend is that as Pr increases N_a and N_0 decrease. For Pr less than about 0.50 the solution changes rapidly with Pr. The solution is not very sensitive to values of Pr once Pr is above about 1.50. The lowering of the vorticity is accompanied by thicker cat's-eyes and larger reflected and incident waves, a familiar result.

It is the change in G above the cat's-eyes that is responsible for the variation of N_a with Pr. Because the solution in the upper linear layer is independent of Pr all the above cases have the same initial conditions at the top of the critical layer. Inside the critical layer the vorticity variation along a streamline is given by $-\overline{Ri}\,\zeta F'$ which is essentially independent of Pr (the function F used here keeps the mean density gradient constant, a restraint independent of Pr). The decrease in N_a then, is due to changes in the mean vorticity along the upper cat's-eye boundary which is in turn determined by G. Figure 14 shows the sequence of functions of G as well as the mean

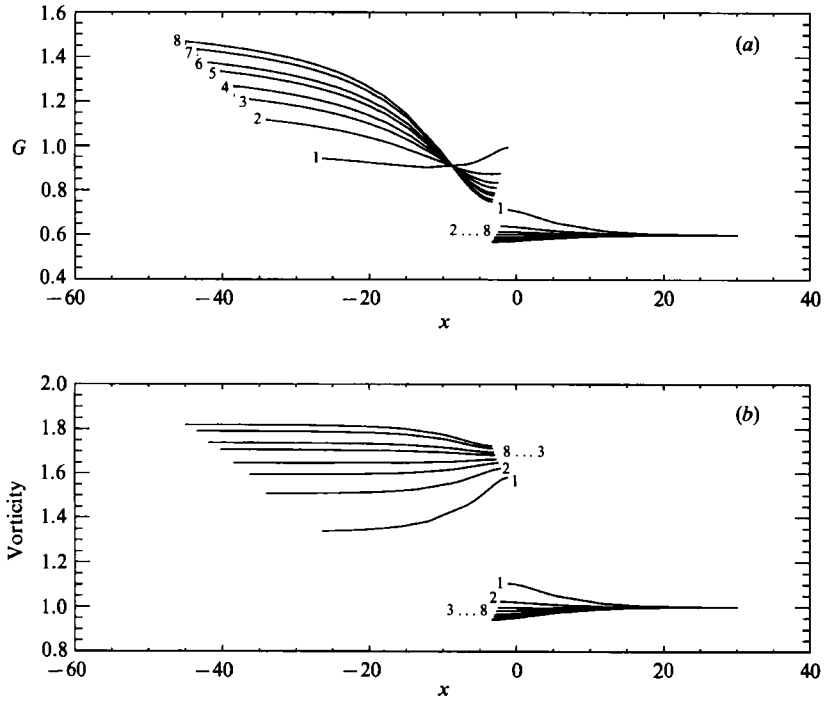

FIGURE 14. Profiles of (a) G and (b) the mean vorticity (average value along a streamline) for different values of Pr plotted as functions of ζ along a vertical line passing through the corner so that the functions above and below the cat's-eyes are separated. $(\overline{Ri}, T, \alpha) = (0.4, 0.01, 0.1)$. Curve 1, $Pr = 0.25$; 2, 0.5; 3, 0.75; 4, 1.0; 5, 1.5; 6, 2.0; 7, 4.0; 8, 8.0.

vorticity for the cases cited in table 4. The mean vorticity at the upper cat's-eye boundary decreases as Pr grows, hence the variation in N_a. As $Pr \to 0$ the mean vorticity at the upper boundary becomes infinite due to the $1/Pr$ term in the equation for G.

The reduction of N_a while $\overline{Ri}$ increases or T decreases is a result obtained for all values of Pr. It leads to the introduction of the function $\overline{Ri}_{\rm crit}(T, Pr)$. A solution exists only if $\overline{Ri} < \overline{Ri}_{\rm crit}(T, Pr)$. The function $\overline{Ri}_{\rm crit}(T, Pr)$ decreases with Pr and increases with T. Figure 15 plots the critical values $\overline{Ri}_{\rm crit}$ as a function of Pr for a few values of T. The critical value is typically in the range 0.4–0.6.

Finally we briefly mention the dependence of the solutions on the horizontal wavenumber α. As α is decreased the flow becomes more hydrostatic and we would expect an improved matching between the linear layers and the critical layer. Numerical results indicate that the solutions break down when α is greater than about 0.3. Below this value the vorticity in the centre decreases very slowly as α decreases, resulting in a slight thickening of the cat's-eyes and larger reflected waves. The effect of decreasing α is generally more pronounced for smaller values of $\overline{Ri}$.

4.4. *Incident, reflected and transmitted waves: relationships*

In the previous section the dependence of the solution on the parameters $\overline{Ri}$, T, Pr and α was discussed in general terms. In this section attention is focused on some of the more physically interesting aspects of the solutions. These include the relationships among the incident, reflected and transmitted waves, the amplitudes of

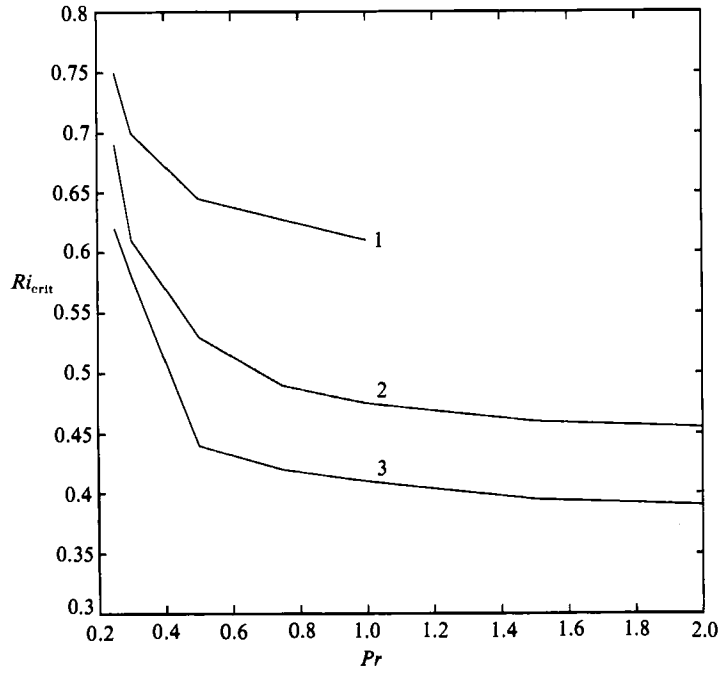

FIGURE 15. $\overline{Ri}_{crit}$ (T, Pr) as a function of Pr for different values of T. A solution exists only if Ri is less than $Ri_{crit}(T, Pr)$. Curve 1, $T = 0.05$; 2, 0.01; 3, 0.002.

the hills below the critical layer and their relationship to the three waves, and finally the resonance positions (locations where the hill amplitude has its minimum value).

If only a single wave mode is present then the amplitude A of the hill which can generate a particular flow pattern is given by $A = [I^2+R^2+2IR\cos(2mz_h+\delta)]^{\frac{1}{2}}$. It depends on the height z_h at which it is located and on the vertical wavenumber m. In particular A lies between $R-I$ and $R+I$. If more than one mode is present these bounds are modified. In most cases computed the mode-one waves dominate the flow so that R usually is larger than I, but because other modes are in general present the lower bound $R-I$ is not usually attained.

In all the cases calculated with only one transmitted mode present the amplitudes of the reflected and incident waves of the first mode were much larger than the amplitudes of the higher modes (~ 5 times larger than the second harmonics). However, when the transmitted wave is small (close to the minimum cutoff value) then the difference between the amplitude of the reflected and incident waves can be very similar for the first two modes. The momentum flux in mode k in the lower linear layer is given by

$$\tfrac{1}{2}(I_k^2-R_k^2)\,km_kL.$$

Thus if R_1-I_1 is sufficiently small in relation to R_2-I_2 the momentum flux in the mode-two waves can be a significant contribution. The sum over all the modes must be negative, equal to the momentum flux in the upper linear layer which is $-\frac{1}{2}T^2\,kmL$.

Consider again the effect of varying the amplitude of the transmitted wave T for $\overline{Ri} = 0.4$, $Pr = 1.1$ and $\alpha = 0.1$. Recall that the solution breaks down at around $T = 0.002$. Table 5 gives the values of the amplitudes of the reflected and incident waves for the first two modes, along with the corresponding momentum fluxes which

T	R_1	I_1	R_2	I_2	Momentum in mode 1 (% of total)	Momentum in mode 2 (% of total)
0.075	0.1923	0.1750	0.0300	0.0360	113.3%	−13.5%
0.050	0.1359	0.1256	0.0193	0.0218	107.9%	−8.0%
0.040	0.1125	0.1047	0.0155	0.0170	105.7%	−5.8%
0.030	0.0893	0.0839	0.0118	0.0124	103.2%	−3.2%
0.020	0.0659	0.0628	0.0084	0.0083	99.7%	0.3%
0.010	0.0421	0.0410	0.0051	0.0046	91.2%	9.0%
0.0075	0.0363	0.0356	0.0045	0.0039	84.5%	15.7%
0.005	0.0312	0.0309	0.0039	0.0033	65.9%	34.2%
0.004	0.0297	0.0296	0.0040	0.0033	41.4%	58.6%
0.003	0.0294	0.0294	0.0043	0.0036	−29.8%	128.6%
0.002	0.0355	0.0358	0.0072	0.0061	−634.5%	710.5%

TABLE 5. The amplitudes of the reflected and incident waves, with the corresponding momentum fluxes for different values of T ($\overline{Ri}$, Pr, α) = (0.4, 1.1, 0.1)

are given as a percentage of the total momentum flux. For large waves the momentum flux in the first mode is much larger than it is in the second mode. As the amplitude of the transmitted wave decreases, the momentum flux in the second mode grows in relation to that in the first mode. A rapid growth in the relative importance of the second harmonics is seen whenever the parameters of the problem are close to a breakdown point. The amplitudes of the waves in the first mode are always much greater than those in the second mode.

Recall that, as discussed in §4.1, the accuracy of the second harmonics is not very good. It is interesting to note that by adding a small-amplitude second harmonic to the transmitted wave (about 0.1 the amplitude of the leading harmonic) and by appropriately choosing the phase difference between the two waves, the momentum flux in the second harmonics below the critical layer can be zeroed out. This zeroing out is accompanied by very small changes to the values of R_1 and I_1, but does significantly change the value of R_1-I_1. Owing to the questions surrounding the validity of the second harmonics below the critical layer this aspect of the solution is not pursued any further. It may be worth noting that, even for the largest cases cited in table 5, R_1-I_1 is smaller than the amplitude of both of the mode-two waves.

Table 6 shows the results of a large number of calculations for different amplitudes T of the transmitted wave and for different values of $\overline{Ri}$. The ratios of the amplitudes of the reflected and incident waves to the transmitted waves of the first modes are given, along with the difference and sum of the two ratios. The latter give the ratio of the minimum and maximum hill sizes to the transmitted wave respectively. The minimum hill size is always significantly smaller than the amplitude of the transmitted wave while the maximum is always significantly larger. For example, for $\overline{Ri} = 0.4$ and $T = 0.05$ the hill must be between 0.2 and 5 times the size of the transmitted wave. For $\overline{Ri} = 0.2$ and $T = 0.05$ the hill must be between 0.4 and 2.5 times the size of the transmitted wave. (Note that if just a single mode were present in the two linear layers then $T^2 = R_1^2 - I_1^2$ and the two ratios $(R_1-I_1)/T$ and $(R_1+I_1)/T$ are the reciprocals of each other.) As T is decreased the ratios of the minimum and maximum hill sizes to T decrease and increase respectively.

Two trends are readily apparent. For a given value of $\overline{Ri}$, as T is increased the ratios $R_1/T, I_1/T$, $(R_1+I_1)/T$ and $(R_1-I_1)/T$ become fairly constant (compared to their rapid changes for small values of T), the first three ratios decreasing while the

$\overline{Ri}$	T	R_1/T	I_1/T	$(R_1-I_1)/T$	$(R_1+I_1)/T$	Res_{cor}	Res_m
0.45	0.075	3.04	2.83	0.21	5.87	0.39	0.26
	0.05	3.40	3.23	0.17	6.62	0.37	0.25
	0.04	3.69	3.54	0.15	7.22	0.36	0.25
	0.03	4.11	3.98	0.13	8.09	0.35	0.25
	0.02	5.08	4.99	0.09	10.07	0.34	0.25
	0.01	9.28	9.32	−0.04	18.60	0.34	0.26
0.4	0.075	2.56	2.33	0.23	4.90	0.36	0.24
	0.050	2.72	2.51	0.21	5.23	0.34	0.24
	0.040	2.81	2.62	0.19	5.43	0.32	0.24
	0.030	2.98	2.80	0.18	5.77	0.31	0.23
	0.020	3.29	3.14	0.15	6.43	0.29	0.23
	0.010	4.21	4.09	0.11	8.30	0.27	0.23
	0.005	6.24	6.19	0.05	12.43	0.27	0.24
	0.004	7.44	7.41	0.03	14.84	0.27	0.24
	0.003	9.79	9.80	−0.02	19.59	0.27	0.24
	0.002	17.73	17.91	−0.18	35.64	0.29	0.25
0.3	0.075	1.90	1.60	0.30	3.50	0.30	0.22
	0.05	1.91	1.62	0.29	3.53	0.28	0.21
	0.02	2.01	1.74	0.27	3.74	0.24	0.21
	0.01	2.11	1.86	0.25	3.97	0.23	0.21
	0.005	2.32	2.10	0.23	4.42	0.23	0.21
	0.001	3.03	2.86	0.17	5.89	0.23	0.21
0.2	0.075	1.48	1.09	0.40	2.57	0.25	0.19
	0.05	1.47	1.07	0.40	2.54	0.23	0.19
	0.02	1.47	1.08	0.39	2.55	0.21	0.19
	0.01	1.49	1.11	0.39	2.60	0.20	0.18
	0.005	1.53	1.16	0.37	2.69	0.20	0.18
	0.002	1.58	1.23	0.36	2.81	0.20	0.19
	0.001	1.63	1.28	0.34	2.91	0.20	0.19
	0.00001	1.95	1.68	0.28	3.63	0.21	0.20
0.1	0.05	1.19	0.647	0.55	1.84	0.19	0.16
	0.02	1.18	0.626	0.55	1.81	0.17	0.16
	0.01	1.19	0.638	0.55	1.82	0.17	0.16
	0.005	1.19	0.649	0.54	1.84	0.17	0.16
	0.001	1.21	0.674	0.53	1.88	0.17	0.16
	0.0001	1.23	0.710	0.52	1.94	0.17	0.17

TABLE 6. The ratios of the amplitudes of the reflected and incident waves, and their sums and differences, to the transmitted waves of the first mode. The distances of the first resonant position below the corner of the cat's-eye and below the matching of the critical and lower linear layers are also shown, as a fraction of vertical wavelength $(Pr, \alpha) = (1.1, 0.1)$.

last one increases. For T fixed the first three ratios all decrease while the last one increases as the Richardson number is decreased.

Also shown in table 6 are the distances of the first resonant position (height where leading mode has amplitude R_1-I_1) below the corner of the cat's-eye as well as below the height where the critical layer and the lower linear layer were matched together. These values are Res_{cor} and Res_m respectively and are given as a fraction of the vertical wavelength in the region of the lower linear layer where the mean wind speed is constant and equal to -1.0. Resonant positions are separated by distances of half a vertical wavelength.

For $\overline{Ri}$ constant Res_m is almost independent of T and increases with $\overline{Ri}$ from about 0.16 for $\overline{Ri} = 0.1$ to about 0.24 for $\overline{Ri} = 0.4$. Res_{cor} shows more variation. It is larger than Res_m (as it must be since the cat's-eye corner is above the matching level) and

increases both with $\overline{Ri}$ and to a lesser degree with T. The difference between Res_{cor} and Res_{m} grows as the parameter values change in such a way that the flow is less linear and the match takes place further below the cat's-eyes. For these cases more of the wave is reflected at the 'bump' in the lower mean wind and the centre of reflection is shifted to this region of the flow. It is interesting to note that all the resonant positions are close to 0.25 (plus multiples of 0.5). This is the value Peltier & Clark (1983) found to be consistent with the resonant amplification of mountain waves observed in their numerical simulations. However, since their simulations were for an isolated mountain rather than a sinusoidal one, the agreement may be fortuitous.

5. Conclusions

For an incompressible, nearly inviscid, stratified fluid, we have considered the behaviour of a spatially periodic internal gravity wave impinging on a critical level from below; transmitted waves, if any, were constrained to satisfy a radiation condition far above the critical level. By a combination of asymptotic and numerical means, we were able to construct steady, nonlinear solutions to this problem over a broad area of parameter space. In contrast to most previous studies (e.g. Maslowe 1972, 1986 or Stewartson 1981) we did not need to assume very weak stratification, nor did we require the waves to be trapped in the vicinity of the critical level. These steady solutions are end states that could result from integration of the nonlinear initial-value problem; it is conjectured that they represent the asymptotic long-time behaviour of the stratified critical level problem, as has proved to be the case for unstratified critical levels.

As usual, the flow consists of a layer of recirculating streamlines, called cat's-eyes, sandwiched between two regions of open streamlines (which are nevertheless governed by nonlinear dynamics near the critical level). The vorticity interior to the cat's-eyes was chosen according to a torque condition, which minimizes the long-term viscous spin-up or spin-down of the vortices. Unlike Maslowe's solutions, these solutions do not have a velocity discontinuity across the cat's-eye boundaries, and hence do not require a viscous boundary layer to complete the solution. In this sense, they are more stable than previous solutions; however, the local Richardson number does fall below 0.25 in some regions near the cat's-eye boundaries, and so the possibility of Kelvin–Helmholtz instability cannot be ruled out. We were able to construct these continuous solutions because we allowed the position of the critical level to shift somewhat, rather than fixing it at the location of the zero wind line of the unperturbed background flow.

Another departure from earlier results is that in our solutions the cat's-eye boundaries have corners, just as in the unstratified case. Maslowe found cornerless solutions because of his choice of where to start the closed-streamline region, together with certain imposed symmetries. In fact, we have shown that similar cornerless solutions can also be found in the absence of stratification. Thus, the presence or absence of corners has little to do with stratification. We did find, though, that with stratification a 'corner condition' must be imposed in order to avoid unphysical discontinuities in vertical velocity.

In contrast to linear theory, the nonlinear critical level can be strongly reflecting; in fact it is over-reflecting, to the extent that there is a transmitted wave. Very weakly stratified critical levels allow a substantial transmitted wave to pass, but a rather moderate increase in stratification (about enough to bring the ambient flow

Richardson number above 0.25) turns them into nearly perfect reflectors. Other things being equal, low-amplitude waves are transmitted less than high-amplitude waves, with amplitude sensitivity becoming more pronounced with increasing stratification.

For the reasons noted in the Introduction, the resonant positions (i.e. the distances below the critical level at which a small forcing can drive a large response) are of considerable physical importance. Strong resonance occurs only if the transmitted wave is weak, a condition that is easy to satisfy if the stratification is not too small. The resonant positions depend on wave amplitude and on the Richardson number, $\overline{Ri}$ of the background flow. They are located approximately $\frac{1}{4}$, $\frac{3}{4}$, $\frac{5}{4}$, ... of a vertical wavelength below the critical layer. They move closer to the critical layer as $\overline{Ri}$ decreases, the first resonant position being about 0.2 wavelengths below the cat's-eye corner for $R = 0.2$ and about 0.3 wavelengths below for $R = 0.4$. For large values of $\overline{Ri}$ the first resonant position is very close to 0.25 wavelengths below the level where the critical layer is matched to the lower linear layer. It is never further than 0.25 wavelengths away and can be as low as 0.16 wavelengths away for very small values of $\overline{Ri}$.

There appears to be an upper bound on the strength of the ambient stratification for which a solution can be found. The breakdown is manifested by small vorticity in the cat's-eyes, and consequent catastrophic thickening of the recirculating region. Solutions were obtained only if $\overline{Ri}$ is less than some critical value $\overline{Ri}_{\mathrm{crit}}(T, Pr)$ which depends on the amplitude T of the transmitted wave and on the Prandtl number Pr. This critical value increases with T and decreases with Pr. There is little dependence on the horizontal wavenumber α as long as it is less than about 0.3. The critical values of $\overline{Ri}$ are typically in the range 0.4–0.6. Our conjecture is that a gravity wave impinging on a too strongly stratified critical level would go through a stage in which a thick layer of fluid is mixed, thus bringing the stratification down to a value which can support a steady state.

The existence of steady solutions such as we have constructed merely shows that it is *possible* for the nonlinear initial-value problem to evolve into a steady, highly reflective state. It does not by any means guarantee that the solutions are physically realizable. This can be probed most effectively by numerical integration of the nonlinear initial value problem. We are not aware of any high-resolution long-term simulations that are conducted in a geometry that permits comparison with our results. The simulations reviewed in Fritts (1984, see his figure 14) do indeed suggest a stratified cat's-eye shape with relatively flat top, bulging bottom, and phase shift between top and bottom, much as seen in our solutions. However, these solutions were not carried out to a steady state, and the critical level was too close to the boundary to permit sensible evaluation of reflection coefficients. The more recent simulations of Winters & D'Asaro (1989) were carried out in a larger vertical domain. However, the incident wave consisted of a pulse of relatively short duration; there was no suggestion of the formation of cat's-eyes, and the incident wave packet was predominantly absorbed near the critical level. There is thus a need for high-resolution long-term simulations of a horizontally periodic wave in a vertically extensive domain. It is to be hoped that the steady-state properties adduced above will be of assistance in guiding such work.

The first author was partially supported by an NSERC (Canada) Postgraduate Scholarship and by the National Science Foundation under grant number NSF ATM343-6049.

REFERENCES

BACMEISTER, J. T. & PIERREHUMBERT, R. T. 1988 On high drag states of nonlinear stratified flow over obstacles. *J. Atmos. Sci.* **45**, 63–80.

BENNEY, D. J. & BERGERON, R. F. 1969 A new class of nonlinear waves in parallel flows. *Stud. Appl. Maths* **48**, 181–204.

BOOKER, J. R. & BRETHERTON, F. P. 1967 The critical layer for internal gravity waves in a shear flow. *J. Fluid Mech.* **27**, 513–539.

BRETHERTON, F P. 1966 The propagation of groups of internal gravity waves in a shear flow. *Q. J. R. Met. Soc.* **92**, 466–480.

BROWN, S. N. & STEWARTSON, K. 1978 The evolution of the critical layer of a Rossby wave. Part II. *Geophys. Astrophys. Fluid Dyn.* **10**, 1–24.

BROWN, S. N. & STEWARTSON, K. 1980 On the nonlinear reflexion of a gravity wave at a critical level. Part 1. *J. Fluid Mech.* **100**, 577–595.

BROWN, S. N. & STEWARTSON, K. 1982 On the nonlinear reflection of a gravity wave at a critical level. Part 2. *J. Fluid Mech.* **115**, 217–230.

FRITTS, D. C. 1984 Gravity wave saturation in the middle atmosphere. A review of theory and observations. *Rev. Geophys. Space Phys.* **22**, 275–308.

GRAHAM, E. W. 1982 On the steady-state relations between disturbances above and below a critical level. *J. Fluid Mech.* **115**, 395–410.

HABERMAN, R. 1972 Critical layers in parallel flows. *Stud. Appl. Maths* **51**, 139–160.

KELLY, R. E. & MASLOWE, S. A. 1970 The nonlinear critical layer in a slightly stratified shear flow. *Stud. Appl. Maths* **49**, 301–326.

KILLWORTH, P. & MCINTYRE, M. E. 1985 Do Rossby wave critical levels absorb, reflect or over-reflect? *J. Fluid Mech.* **161**, 449–492.

LAMB, K. G. 1989 Nonlinear internal gravity wave critical layers. Ph.D. thesis, Princeton University.

MASLOWE, S. A. 1972 The generation of clear air turbulence by nonlinear waves. *Stud. Appl. Maths* **51**, 1–16.

MASLOWE, S. A. 1973 Finite-amplitude Kelvin–Helmholtz billows. *Boundary-Layer Met.* **5**, 43–52.

MASLOWE, S. A. 1986 Critical layers in shear flows. *Ann. Rev. Fluid Mech.* **18**, 405–432.

MOORE, D. W. & SAFFMAN, P. G. 182 Finite-amplitude waves in inviscid shear flows. *Proc. R. Soc. Lond.* A **382**, 389–410.

PALMER, T. N., SHUTTS, G. J. & SWINBANK, R. 1986 Alleviation of a systematic westerly bias in general circulation and numerical weather prediction models through an orographic gravity wave drag parameterization. *Q. J. R. Met. Soc.* **112**, 1001–1039.

PELTIER, W. R. & CLARK, T. L. 1983 Nonlinear mountain waves in two and three spatial dimensions. *Q. J. R. Met. Soc.* **109**, 527–548.

STEWARTSON, K. 1981 Marginally stable inviscid flows with critical layers. *IMA J. Appl. Maths* **27**, 133–175.

WINTERS, K. & D'ASARO, E. A. 1989 Two-dimensional instability of finite-amplitude internal gravity wave packets near a critical level. *J. Geophys. Res.* **94**, 12709–12719.